International journal
for science, technics and
innovations for the industry

MACHINES TECHNOLOGIES MATERIALS

YEAR XV Issue 7 / 2021 ISSN PRINT 1313-0226
ISSN WEB 1314-507X



Published by
Scientific technical
Union of Mechanical Engineering

MACHINES. TECHNOLOGIES. MATERIALS

INTERNATIONAL SCIENTIFIC JOURNAL

ISSN PRINT 1313-0226, ISSN WEB 1314-507X, YEAR XV, ISSUE 7 / 2021

INTERNATIONAL EDITORAL BORARD

EDITOR IN CHIEF:

Georgi Popov	Technical University of Sofia	BG

MEMBERS:

Abdrakhman Naizabekov	Rudny industrial institute	KZ
Ahmet H. Ertas	Bursa Technical University	TR
Albert Albers	Karlsruhe Institut of Technology	DE
Andrzej Golabczak	Lodz University of Technology	PL
Andrzej Huczko	Warsaw University	PL
Dimitar Karaivanov	University of Chemical Technology and Metallurgy, Sofia	BG
Emilia Abadjieva	Akita University	JP
Erdem Camurlu	Akdeniz University, Antalya	TR
Eugen Sheregii	University of Rzeszow	PL
Franz Haas	Graz University of Technology	AT
Galina Nicolcheva	Technical University of Sofia	BG
Gennadii Bagliuk	Institute for Problems of Materials Science NAS of Ukraine, Kiev	UA
Georgii Raab	Ufa State Aviation Technical University	RU
Gregory Gurevich	Shamoon College of Engeeniring, Ashdod	IL
Hiroyuki Moriyama	Tokai University, Hiratsuka	JP
Idilia Batchkova	University of Chemical Technology and Metallurgy, Sofia	BG
Ivan Kralov	Technical University of Sofia	BG
Ivan Kuric	University of Zilina	SK
Julieta Kaleicheva	Technical University of Sofia	BG
Katia Vutova	Institute of Electronics, Bulgarian Academy of Sciences	BG
Maria Nikolova	Angel Kanchev University of Ruse	BG
Natasa Naprstkova	Jan Evangelista Purkyne University in Usti nad Labem	CZ
Oana Dodun	Gheorghe Asachi Technical University of Iasi	RO
Ognyan Andreev	Technical University of Sofia	BG
Predrag Dasic	High Technical Mechanical School of Trstenik	RS
Rasa Kandrotaite	Kaunas University of Technology	LT
Raul Turmanidze	Georgian Technical University, Tbilisi	GE
Roumen Petrov	Ghent University	BE
Sergey Dobatkin	National University of Science and Technology "MISIS", Moscow	RU
Souren Mitra	Jadavpur University, Kolkata	IN
Svetlana Gubenko	National Metallurgical Academy of Ukraine, Dnipro	UA
Vedran Mrzljak	University of Rijeka	HR
Wu Kaiming	Wuhan University of Science and Technology	CN

TECHNICAL EDITORS:

M. Sc. Eng. Radoslav Daskalov, M. Sc. Eng. Oleg Mihailov

Scientific and technical union of mechanical engineering
108 R. S. Rakovski str., Sofia, Bulgaria
www.stumejournals.com, office@stumejournals.com

C O N T E N T S

MACHINES

The immovable mixers for the dosing of the substrate on the biogas plants
Milica Josimovic, Slavica Prvulovic, Sasa Jovanovic, Dragica Radosav 252

Thin layer activation method. Potential applications and benefits for the food processing industry.
Delyan Gospodinov, Vilhelm Hdjiiski, Stefan Dishliev, Severin Traian-Lucian 256

TECHNOLOGIES

Pitting factor in use of galvanostatic pulse method for measuring the corrosion rate of reinforcement in concrete
Davor Grandić, Ivana Štimac Grandić 259

The application of rapid prototyping in the studing of samples of filtering materials based on woven nets
Aliaksandr Ilyushchanka, Iryna Charniak, Aliaksei Kusin, Vecheslav Kaptsevich, Ruslan Kusin,
Nataliai Rutkovskaya, Dmitry Shamal 264

Testing of technology for joining materials in the automotive industry
Emil Evin, Ján Viňáš, Dušan Sabadka 267

MATERIALS

Estimation of the elasticity module of Al-Si alloy samples in cast and deformed states by the frequency spectrum of sound vibrations
Vladislav Kaverynskyi, Zoya Sukhenko , Gennadii Bagliuk 271

The nanostate factor in the technology of polymer nanocomposites
Avdeychik Sergey, Goldade Victor, Antonov Alexander, Struk Vasily, Klochko Pavel 275

State and prospects of application of plastically deformed nanostructured metals, alloys, and sprayed coatings
Syzonenko Olha, Dubovyi Oleksandr, Makrukha Tetiana, Karpechenko Anton, Bobrov Maksym, Torpakov Andrii 279

Investigation of the causes of corrosion of galvanized steel pipes used for hot water supply
Rasa Kandrotaitė Janutienė, Darius Mažeika 283

Recent applications of nanoparticles in wood-based panels
Nadir Ayrilmis 287

The immovable mixers for the dosing of the substrate on the biogas plants

Milica Josimovic, Slavica Prvulovic, Sasa Jovanovic, Dragica Radosav
University of Novi Sad, Technical Faculty "Mihajlo Pupin", Zrenjanin, Serbia
Email: prvulovicslavica@yahoo.com

Abstract: *In this paper the solutions, types and groups of immovable mixers for the dedicated biogas power plants, as well as the connections (calculation) of the pipes for the transport of the substrata from the mixer to the digester are presented.*
The continuous feeding on biogas devices represents the challenge with which every producer of the electricity, more precisely, of the biogas device, is faced.
Apart from numerous research, the feeding with the immovable mixers for the dosing of the mass, turned out to be an adequate and the most economical solution.
The using of the immovable mixers with the direct inserting of the mass into the digester represents the most effective way of feeding the biogas devices which have the need for the solid matter and it does not have the liquid preparation. The new way of feeding is ideal for the biogas devices which have diagonal mixers in the digesters and which can follow the dosing of the immovable mixers.
Keywords*: IMMOVABLE MIXER, SUBSTRATUM, BIOGAS DEVICE, DIGESTER*

,

1. Introduction

The biogas plant is a renewable energy source and it has its place in the modern energetics of the 21st century. It enables a stable supply of electricity and heat, without affecting the environment with emissions, and it has a long-term support of the European Union [1-3]. In addition to the primary task of energy production, biogas plants also have a role in protecting the environment, not only by reducing the greenhouse effect, but also by eliminating agricultural production waste and biodegradable municipal waste. The controlled process of anaerobic fermentation is the basic technology on which the biogas plant is based [4-6]. Anaerobic fermentation is a biochemical process in which complex organic compounds are decomposed by the action of different types of bacteria in anaerobic conditions (without the presence of oxygen) and the organic matter is converted to energy-rich biogas by heating and mixing. The properties and composition of biogas depend on the type of substrate, the method of production, the type of plant, the temperature at which the process took place, the duration of hydraulic retention, the volume of the digester and other factors [6-9]. The energy value of biogas is chemically bound in methane. The average calorific value of biogas is about 6.5 MJ / m3.

Raw materials for biogas production can be: animal manure, green mass (plants), corn silage, expired food products (if hygienically safe), rotten seeds, beet pulp, molasses, fruit pulp, residues from vegetable and fruit processing, seeds, peel, fallen fruit, leftovers, residues from the beer industry, residues from milk and cheese production, residues from oil production, etc.[1, 10, 11]

Biogas Composition: methane CH4 ca. 50 - 75%, carbon dioxide CO2 ca. 25 - 50%, nitrogen N2 ca. 0 - 3%, hydrogen H2 ca. 0 - 1%, oxygen O2 ca. 0 - 1%, hydrogen sulfide H2S ca. 0 - 2%. The composition of the biogas is generally affected by the substrates used, the fermentation process and various technical performances. The goal of the plant is the production and delivery of electricity in the public network, as well as the use of thermal energy as an accompanying product for internal purposes [5, 7, 10].

Biogas installation is a clean and logical way to generate and sustain energy from agricultural resources.

The biogas producer strives to produce more energy with a minimum amount of mass input [10,12].

2. Material and method

2.1 Substrate preparation

The method and scope of substrate preparation, on the one hand, affect the general usability of the substrate in terms of the content of undesirable substances, so that they have a direct impact on the availability of technical equipment of the plant. In addition, an adequate preparation process can positively affect the course of the fermentation process, and thus the utilization of the energy potential of the substrates used. With the fragmentation of the substrate, the substrate surfaces are prepared for biodegradation and thus for methane production.

In principle, one can start from the fact that with the increased degree of fragmentation, the rate of biodegradation increases, but not necessarily the gas yield. Among other things methane production is influenced by fermentation time and the degree of fragmentation. Therefore, great attention must be paid to the use of adequate technical devices.

The solid substrate shredder can be installed externally before feeding into the pit, piping or fermenter. For this, shredders, mills, crushers as well as shafts and augers with tearing devices and blades are available.

Fragmentation can be done, among other things, by means of separate mixers with an integrated shredding device in the pit which is connected upstream from the fermenter in the process line [13].

There are stationary mixers with vertical coils and capacities from 10 to 80 m³, which will be explained in great detail in this paper.

2.2 Technical description of vertical mixers

So far, it has been shown that the company "Trioliet" has a solution for the most economical and above all adequate technology for feeding digesters. Trioliet vertical mixers type SOLOMIX (Fig. 1, Table 1) are excellent for feeding biogas plants [13].

The machine is equipped with one drain door as standard, it contains two augers for mixing with a planetary drive mechanism driven by one or two electric motors, four height-adjustable brackets with the option of installing scales for different installation options and two manually operated counter knives (Figure 2).

There are:

1. Mixers with 15 mm winding / 18 mm auger wings (1200 - 2000)

2. Mixers with 22 mm thread / 25 mm auger wings (from 2400)

Trioliet vertical mixers are excellently suitable for feeding biogas plants. All Trioliet stationary mixers have a highly stable auger supported by the integrated frame. Consequently, all forces extended on the mixing auger are directly taken up by the frame. This design relieves the mixing chamber bottom and the gearbox. The compact and closed planetary drive ensures a constant and controlled rotating movement of the cutting mixing auger. The auger runs in a maintenance-free conical roller bearing at the top and a sinter slide bearing at the bottom. The optimum auger shape ensures quick and homogenous mixing at a low power requirement. Just above the bottom, at the lower end of the mixing chamber wall where the pressure on the wall is highest, a special Trioliet wearing ensures stability and a long service life.



Fig. 1. *Fixed dosing basket with mixers [13]*



Fig.2. *Interior design of the dosing basket [13]*

There are mixers that provide:

(A) Feeding in standing digesters.

(B) Feeding into semi-underground soil digesters.

(C) Feeding into underground digesters.



Fig.3. *Types of mixers [13]*

The substrate dosing basket on the biogas plant is made of steel and protected with epoxy coatings. Total working volume V = 8m^3, maximum silage tonnage Q = 6.8t. The basket is equipped with a spiral for removing silage and a spiral for overturning and dispersing it. Basket dimensions (Length x Width x Height): 7.5 x 2.5 x 2m.

In Table 2, the dimensions of the Triolet for the existing gas plant are given

Table 1*: SOLOMIX 2 basket types and dimensions*

Type Solomax 2	1200	1600	2000	2400	3000	3200	4000
Capacity (m^3)	12	16	20	24	30	32	40
Length (m)	4,21	4,6	5,2	5,72	5,72	6,56	6,56
Length with motors (m)	5,24	5,59	6,28	-	-	-	-
Width (m)	2,15	2,29	2,44	2,44	2,44	2,80	2,80
Width with motors (m)	-	-	-	3,67	3,67	3,84	3,84
Height (m)	2,55-2,85	2,85-3,15	2,85-3,15	2,77-3,07	3,35-3,65	2,75-3,05	3,35-3,65
Weight (kg)	3.400	4.300	5.400	6.400	7.600	9.400	10.000
Maximum load (kg)	6.000	8.000	10.000	12.000	15.000	16.000-20.000	20.000
Number of coil blades	4	5	5	6	6	9	9
Coil diameter	Ø1500	Ø1700	Ø1960	Ø2200	Ø2200	Ø2660	Ø2660
Electrical installation required	Soft-start device	Soft-start device	Soft-start device	Soft-start device	Soft-start device	Soft-start device	Soft-start device
Required power of electric motor	15	22	30	2x15	2x18.5	2x22 2x30	2x30

Table 2: *Triolet dimensions for an existing gas plant*

Triolet	Value	Unit
Length	6558	mm
Width	2792	mm
Height	3643	mm
Total volume	40	m^3

Triolet is used for receiving and mixing fresh matter - substrate. It contains two devices for mixing freshly introduced substrate and each of them has 9 knives.

Two electric motors are used to drive the mixer, each with a power of 30 kW. The basket also includes a helical conveyor. The first on the pull-out is the horizontal Ø300mm, and the length is 3000mm, whose drive is an electric motor with a power of 5.5kW, the number of revolutions of the drive is 56. The second vertical is the total length of 7900 mm, Ø300mm. The third is oblique and it is inserted into the fermenter at an angle of 45 ° in relation to the horizontal, its length is 2500mm and Ø300mm, it is powered by an electric motor with a power of 5.5kW and it is in a special version [13].

3. Results of research and discussion

The location of the mixer is within the biogas plant. A universal system for receiving silage from the Triolet basket with the addition of liquid from the previous thickener and transport with a screw pump is given. Input data is obtained by the user depending on the needs of the plant. In addition to the capacity and other input parameters, the required pipeline diameter must be calculated with the length of the section for supplying the Premix System (devices for crushing and mixing various solids with liquid) [12].

The mass from the mixer basket is inserted with a spiral into the PreMix system. The SOLOMIX 2 basket is equipped with a measuring scale, a force meter and in this way the daily feeding doses are determined. The speed and operating time of the substrate dosing system is harmonized with the operation of the existing plant and the drawing capacity of the centrifugal pump in the pumping station.

3.1 Determination of pipeline parameters for substrate transport from baskets to digesters (2)

The tube DN200, Ø200 SDR17 made of polyethylene PEHD is acquired. The thickness of the wall of the tube is 11.9 mm.
The necessary volume- flow of the mass is

$Q_v = 35 m^3/h = 0.0097\ m^3/s$

For the acquired tube, the velocity of the circulation is:

$$v = \frac{Qv*4}{d^2*\pi} = \frac{0.01*4}{0.176^2*\pi} = 0.41 \text{ m/s}$$

The fall of the pressure at the section whose length is 30 m is:

$$\Delta p = \rho*\lambda*\frac{L}{d}*\frac{V^2}{2} = 990.9*0.013*\frac{0{,}41^2}{2} = 185 \text{ Pa} = 0.0018 \text{bar}$$

In the table 3 are given the results of the calculation of the pipeline-substratum.

Table 3: *The results of the calculation of the pipeline- substratum*

Working conditions		
Working medium		Ferment - Substratum
A state of matter		Liquid
Volume- flow	m^3/h	35.0
The flow of mass	kg/h	34650
Density	kg/m^3	990.919
Dynamic viscosity	10^{-6} kg/ms	1.5
Kinematic viscosity	10^{-6} m^2/s	0.002
The elements of the pipeline		
The mark of the pipeline		PE HD - Substratum
The form of the pipe		Round pipe
Number		1
The dimensions of the pipeline	SI	The diameter of the pipe D in mm: 200.0
		The length of the pipe L in mm: 30.0
The results of the calculation		
Velocity	m/s	0.41
Reynold's number		9.346E+07
The type of the circulation		turbulent
Roughness	mm	0.03
Abrasion coefficient		0.013
Ceta value		7.778
The fall of the pressure	bar	0.0018

4. Conclusion

The paper describes the significance and application of the Triolet Type Solomax 2 mixer, as part of a biogas plant. The selection of a

mixer of appropriate capacity for feeding PreMix systems and existing digesters was performed, as well as the calculation of pipeline parameters for substrate flow.

The conclusion of this paper is that using stationary mixers with direct injection of mass into the digester is the most efficient way of feeding biogas plants that need solids. The new feeding method is ideal for biogas plants that have inclined mixers in digesters and that can monitor the dosing of the immovable mixers.

The advantages of these systems are seen in the fact that they do not require the continuous servicing of the basket itself, they are mounted easily and fast, they have the long-term duration.

5. References

[1] F.S. Nayal, A. Mammadov, N.Ciliz, Environmental assessment of energy generation from agricultural and farm waste through anaerobic digestion, Journal of Environmental Management,184, 389-399 (2016).

[2] M. Milani , L. Montorsi, , M. Stefani, An integrated approach to energy recovery from biomass and waste: Anaerobic digestion-gasification-water treatment, Waste Management and Research, 32, 7, 614-625, (2014).

[3] G. Markou, M. Brule, A. Balafoutis, et al., Biogas production from energy crops in northern Greece: economics of electricity generation associated with heat recovery in a greenhouse, Clean Technologies and Environmental Policy, 19, 4, 1147-1167, 2017.

[4] B. Manganelli, Economic feasibility of a biogas cogeneration plant fueled with biogas from animal waste, Advanced Materials Research, 864-867, 451-455, 2014.

[5] A. Abusoglu, A. Anvari-Moghaddama, J.M. Guerro, Producing bio-electricity and bio-heat from urban sewage sludge in Turkey using a two-stage process, 5th International Conference on Power Generation Systems and Renewable Energy Technologies, Istanbul, 26-27 August, 302-306, (2019).

[6] ACHINAS, S., MARTHERUS, D., KROONEMAN, J., EUVERINK, G.J.W.: Preliminary assessment of a biogas-based power plant from organic waste in the North Netherlands, Energies, 2019, Vol.12, No 21, pp.122-140.

[7] M. Prakash, A. Sarkar, J. Sarkara, S.S. Mondal, J.P. Chakraborty, Proposal and design of a new biomass based syngas production system integrated with combined heat and power generation, Energy, 133, 986-997, (2017).

[8]F. Patania, A. Gagliano, Nocera, A. Galesi, Feasibility study of biogas in CHP plant for a pig farm, Renewable Energy and Power Quality Journal, 1, 10,196-201, 2012.

[9]T. Methling, N. Armbrust, T. Haitz, et al., Power generation based on biomass by combined fermentation and gasification - A new concept derived from experiments and modelling, Bioresource Technology, 169, 510-517, 2014,.

[10] S. Prvulovic, J.Tolmac, M.Joksimović, D. Dragicevic, Biogas Equipment for Electricity and Heating, Scientific Technical Review, 70,1,17-20, (2020).

[11] M. Lantz, The economic performance of combined heat and power from biogas produced from manure in Sweden - A comparison of different CHP technologies, Applied Energy, Vol. 98, pp. 502-511, (2012)

[12] Project documentation of biogas power plant for wastewater treatment, Zrenjanin, 2019.

[13] https://www.trioliet.com/products/stationary-feed-mixers-for-biogas/biogas-solomix-2, Data of last access: 12/05/2021.

.

Thin layer activation method. Potential applications and benefits for the food processing industry.

Delyan Gospodinov[1,*], Vilhelm Hdjiiski[1], Stefan Dishliev[1], Severin Traian-Lucian[2]
University For Food Technologies, Plovdiv, Bulgaria[1]
"Stefan cel Mare" University of Suceava, Suceava, Romania[2]
dgosp@abv.bg

Abstract: *Mechanical wear, corrosion and erosion of the structural materials in machines and apparatus are destructive processes which cause worsening of their basic operational characteristics throughout their life cycle. As a result, the technological equipment undergoes loss of efficiency and reliability. It becomes unsafe from hygienic point of view. The expenses needed for its maintenance increase significantly as the time passes. Its economical efficiency decreases as well. Materials which are in direct contact with food products can also transmit metallic ions or low molecular compounds to the processed food products – a process which is known as "migration". Thin Layer Activation (also known as Surface Layer Activation) is an unique, efficient and innovative radiation based method used for conducting of comprehensive studies on surface degradation of materials. It allows real-time measurements of wear intensities with exceptionally high sensitivity within the scope of several ηm/h (or μg/h). The article reviews the essential principles of the Thin Layer Activation Method (TLA Method), describes its applications, capabilities and advantages. Possible uses in food processing industry are assessed and potential benefits from its implementation are discussed. Technological equipment in food processing industry includes machines and apparatus for production and processing of food products and liquids, packaging equipment, sanitation equipment, equipment for refrigeration and maintaining of certain environmental conditions, transportation equipment and auxiliary tools and equipment.*
Keywords*: WEAR, CORROSION, TECHNOLOGICAL EQUIPMENT, FOOD PROCESSING INDFUSTRY, THIN LAYER ACTIVATION METHOD, REVIEW*

1. Introduction

Mechanical wear, corrosion and erosion of the structural materials are destructive processes which cause worsening of their basic properties. As a result, the technological equipment undergoes loss of efficiency and reliability. It becomes unsafe and the expenses needed for its maintenance increase as the time passes. Its economical efficiency decreases as well.

Deterioration of surfaces which are in direct contact with food products and liquids in the machines and apparatus in food processing industry causes the release of particles of metallic and non metallic nature in the treated products. These particles can undergo chemical interaction with the food products forming new compounds and contaminating the products. Subsequent consumption of the contaminated food products can pose a long-term health risk for the end users.

The manufacture of food products is a process requiring the establishment and maintaining of specific conditions, such as high pressure and high temperature, needed for sustaining of certain biochemical reactions. The food products as well as the auxiliary substances used in their manufacture are most commonly chemically aggressive towards the structural materials. Factors such as pressure and temperature in some cases amplify the negative effects and accelerate the process of surface degradation. Chemical and biochemical agents used for sterilization and sanitation of the equipment are even more aggressive and destructive towards the materials.

Mechanical loadings and friction also lead to the release of metallic and non metallic particles in the processed food products as a result of surface wear. Components such as knives, molds, shafts, bearing, pistons, instruments for extrusion, moving parts in pumps, moving parts in refrigeration equipment, etc., are all subjected to cyclic forces with substantial magnitudes. Cavitation also causes significant wear in the pipe systems, pumps, heat exchangers and so on.

Detailed studies of the processes of wear, corrosion and erosion in the food processing equipment are of a great importance and significance [1, 2]. The information regarding the mechanisms of the surface degradation as well as the influential factors can serve the designers and engineers in favour of creation of new better equipment with higher efficiency, reliability and safety characteristics with much longer operational expectancy. The existing equipment can also be improved and its life extended.

Presently there are several widely used methods for assessment of the wear of the materials which can be divided into a group of methods which allow real-time measurement of the wear and a second group of methods which do not provide chance for real-time measurements.

Real-time measurement methods include the use of different sensors such as capacity sensors, eddy-current sensors or distance sensors. Monitoring the content of the wear particles in lubricant fluids is also an option.

The second group of methods consists of measuring and comparing the mass or the volume of a machine part before and after wear occurrence. These parameters are related to the density of the material [3]. Another approach for assessment of the wear consists of measuring certain geometric parameters of the wear mark and then calculating the wear volume.

All these methods however do not provide the opportunity for precise enough determination and assessment of the wear and its intensity. Certain disadvantages and specifics of their implementation do not allow the achievement of high accuracy measurements with low enough resolution. Thin Layer Activation (TLA), which is also known as Surface Layer Activation (SLA) is a radiation methods for studying of the surface deterioration of the materials. It consists of activation of a thin layer of a surface and subsequent measurement of its activity. The wear is then determined by the decrease of the activity as a result from the loss of material from the activated surface.

2. Basic methods for activation of materials

There are essentially two basic ways for activation of a material by creation of particles of different radionuclides in them. These ways are the neutron activation and ion beam activation.

Neutron activation is conducted by bombardment of a material with thermal neutrons. Neutrons penetrate trough the entire volume of the bombarded target of specific material. As a result of the occurring nuclear reactions, a homogenous bulk activation is achieved with the part having uniformly distributed activity. Typically a fission reaction within a nuclear reactors is used as a source of neutron flux needed for the activation process. Natural sources of neutrons such as ^{252}Cf could also be used as well as sources with ^{241}Am in combination with ^{9}Be.

Austenitic non magnetic stainless steel is the most widely used material in the food processing industry. It contains additional elements such as chromium, nickel, titanium, manganese and

others, with iron serving as basis for its formation. Typical carbon content of the most frequently used steel alloys in food processing industry is between 0,1% and 0,5%. Neutron activation of a austenitic stainless steel would produce radionuclides such as ^{55}Fe, ^{59}Fe, ^{51}Cr, ^{59}Ni, ^{63}Ni, ^{65}Ni, ^{56}Mn, ^{60}Co and ^{51}Ti. Neutron activation is not the preferred option for wear studies since it results in the activation of the entire part. This significantly reduces the sensitivity of the measurements since the decrease of the activity is difficult to be detected as it makes almost insignificant portion of the total activity [4].

Thin Layer Activation method mostly relies on ion beam activation approach which consists of bombarding the target material with high energy charged particles such as protons, deuterons and alpha particles. Unlike neutrons, charged paricles penetrate and lose energy within few millimeters in the bombarded material. Some of them interact with the electrons of the atoms while others interact with the nuclei of the atoms which results in the formation of radionuclides. An example of such nuclear reaction is the formation of ^{56}Co followed by the ejection of a neutron by bombarding ^{56}Fe with protons as follows: ${}^{56}_{26}Fe_{30} + p \rightarrow {}^{56}_{27}Co_{29} + n \cdot$

Unlike neutron activation approach, which leads to a bulk activation of the entire parts, ion beam bombardment results in an activation of a surface layer only. The achieved activity is higher at the exterior of this layer and lower as the depth increases [4, 5, 6].

Activation of all metals and alloys which are of significance for the food processing industry is achievable by using ion beam [4, 5, 6, 7, 8]. Activation does not affect the basic properties of the materials. Typically cyclotrons and linear particle accelerators are used for generation of high energy ion beams.

Polymer based materials such as plastics as well as some ceramics cannot be activated directly by exposing their surfaces to high energy streams of charged particles. These materials are activated by being impregnated with radioactive nuclei mostly by different ways of sputtering [4, 9, 10]. Usually, metallic target is activated by being bombarded either with neutrons or with high energy charged particles such as protons, deuterons and alpha particles. The activated target is then subjected to a treatment, so it can be used as an ion sputtering cathode. Heavy radioactive ions from the cathode are then accelerated with linear accelerator, so they can be implanted into the surface layer of the studied material [4, 10].

3. Thin Layer Activation – method essentials

The Thin Layer Activation (TLA) method consists of an activation of a thin layer of a surface which is subjected to friction and wear. The wear is determined by measuring the reduction of the activity of the activated layer (figure 1). The decrease of the activity as a result of the natural radioactive decay is accounted by calculating the relative activity A_R as follows:

$$A_R = \frac{A_M}{A_0 e^{-\mu t}}$$

where:

- A_M – measured activity,
- A_0 – initial activity after activation,
- μ – constant of radioactive decay,
- t – time since activation.

The wear is a function of the decrease of the relative activity.

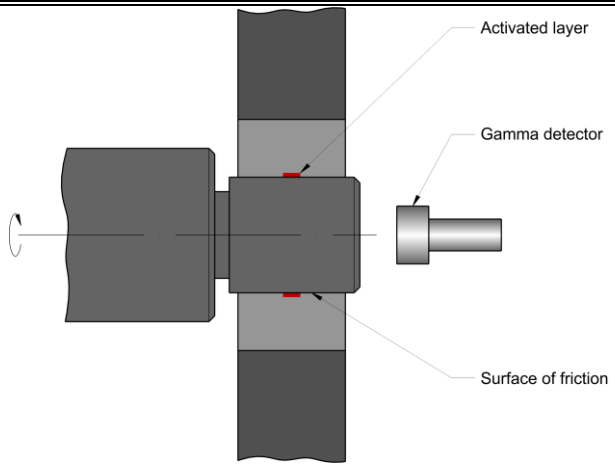


Fig. 1 *Basic principle of the Thin Layer Activation method.*

There are essentially two approaches to assess the wear of the surfaces by implementing TLA. One is to conduct direct measurement of the activity of the surfaces which are activated and are subjected to influences which cause their degradation. This approach requires gamma detection equipment to be positioned at close proximity to the studied surfaces, which is not always possible due to various limitations. In some cases gamma rays emitted from the activated surfaces have to be detected trough thick metallic walls and from significant distance. This requires higher initial values for activity to be achieved when activating the surfaces, which poses additional concerns from radiation safety point of view. Machine parts subjected to friction release heat which could cause heating of the gamma detection equipment which could result in worsening of its accuracy and reliability – results could be compromised.

Second approach involves determination of the content of radioactive particles in the lubricating fluids. As a result from wearing and surface degradation, radioactive particles from the activated surfaces are released in the lubricating fluids and are being carried away. By detecting the presence of these particles in the stream, the process of wear can be "observed" in real-time with accuracy in the scope of several ηm per hour or μg per hour [4]. The particles serve as a radiotracer elements. Application of this approach does not require gamma detection devises to be placed at close proximity to the surfaces whose degradation is being studied. Lower initial activities are required from the process of activation. An alternative is to use filtering system which captures and collects the radioactive tracing particles in the stream. Gamma detection equipment therefore can be mounted at the filter. The accuracy and sensitivity in this case is limited by the efficiency of the filter as it cannot capture all radioactive particles released in the stream as a result from surface degradation.

4. Advantages of Thin Layer Activation method

TLA has many distinguishable advantages in comparison to the traditional methods for studying the degradation of surfaces of structural materials as a result from corrosion, erosion and mechanical wear [4, 5, 10, 11, 12].

It can be used to study the degradation process of specific surfaces or even selected areas within the surfaces – something that cannot be done by using more common methods. Studies of simultaneous wear of multiple surfaces which undergo friction can be studied in real-time. Comparing weight or volume of parts is the most popular method for assessing the wear. This method however, does not provide an opportunity to determine the wear of selected surface of interest. Only total loss of material can be determined.

TLA also allows conducting of non-destructive monitoring of the wear of specific parts in functional technological equipment from distance while the equipment is still working. In this case it is

not necessary to interrupt its operation or disassemble it, in order to reach the studied parts. Wear intensities as low as several ηm/h or μg/h can be easily detected – a sensitivity which cannot be achieved with traditional methods due to number of limitations [4]. Since gamma rays penetrate trough different materials and can be easily detected, TLA enables studies of the wear of machines parts which are hard to access.

5. Conclusion. Potential applications and benefits for the food processing industry.

Food processing industry encloses many sub-level industries ranging from the manufacture and processing of food products and liquids to the production and supplying of individual machine parts to be added into the technological equipment. This also includes the production of equipment for refrigeration and maintaining of specific environmental conditions essential for long-term storage and transportation of food products as well as packaging equipment and tools. Manufacturing and processing of products which are intended for consumption is done under strict requirements for sanitation and hygiene, thus industries providing the necessary tools and equipment are also to be considered as part of the food processing industry.

The aim of the engineers creating modern processing equipment and tools for the food industry is to design machines and apparatus which are more reliable, safer, economically efficient, has longer operational expectancy, consumes less energy, is easy to maintain, easy to clean and sanitize, is less likely to contaminate the processed products and the environment and has higher productivity. Destructive processes such as corrosion, erosion and mechanical wear affect negatively all the functional characteristics of the technological equipment. Although these processes cannot be avoided, a comprehensive knowledge on the mechanisms of their occurrence as well as the factors which affect them can help the modern engineers in the goal for optimization and improvement of the technological equipment, so the negative effects are minimized and the wear intensity reduced. Thin Layer Activation method provides an excellent opportunities for performing of comprehensive studies of the wear and corrosion in the machines and apparatus in food processing industry.

Migration is a process specific to the food processing industry. It is a hazardous phenomenon consisting of different particles being released in the food products and liquids as a result of the degradation of the surfaces which are in direct contact with these products. Metals tend to release metallic ions in the food products while plastics and other polymer materials such as rubber and paper normally release low-molecular weight compounds. Some of these particles can be chemically neutral with respect to the food products, while others can undergo chemical interaction forming additional compounds within the food products. All these products of migration process are subsequently consumed along with the food and find their ways into the human organism where they can pose long-term health risk. The process of migration is intensified when certain conditions such as high temperature and/or high pressure combined with chemical aggressiveness are met during biochemical and thermal treatments such as boiling, frying, baking and fermentation. Migration occurs not only in food processing equipment, but in food packaging as well.

Thin Layer Activation method is an excellent opportunity for conducting a comprehensive studies of the process of migration. Considering the detection abilities of the modern gamma sensing technologies and spectral analysis equipment, one such study using TLA techniques would achieve sensitivity that cannot be matched by other methods, enabling real-time monitoring of the process.

Development and technological improvements as well as increasing availability of ion beam generation equipment make Thin Layer Activation method more accessible for researchers across the globe.

6. References

1. G. Mishev, V. Rupetzov, M. Simov, Possibilities for Increasing the Resource of Injection Molds, Trib. J. BULTRIB, 4, 69-74, (2014)
2. V. Rupetsov, L. Kolaklieva, V. Chitanov, M. Angelov, R. Raychev, Z. Zlatanov, Ch. Pashinski, Deposition and tribomechanical study of nanolaminate Ti/TiN/AlTiSiN/(AlTiSiN/TiAlSiN)n/AlTiSiN hard coating, IOP Conf. Series: Materials Science and Engineering, 618 (2019) 012047, doi:10.1088/1757-899X/618/1/012047, SJR 0.192
3. D.M. Kennedy, M.S.J. Hashmi, Methods of wear testing for advanced surface coatings and bulk materials; J. of Mat. Proc. Tech., 77, (1998) 246–253
4. International Atomic Energy Agency, Radiotracer Technologies for Wear, Erosion and Corrosion Measurement, IAEA-TECDOC-1897, IAEA, Vienna, (2020)
5. M.C. Garcia-Alonso, G. Macchi, C. Brugnoni, M.F. Stroosnijder, Electrochemical release testing of a stainless steel in a glucose solution using thin layer activation, Corrosion Science, 44 (1), 129-143, (2002)
6. R.C. Saxena, J. Biswal, H.J. Pant, J.S. Samantray, S.C. Sharma, A.K. Gupta, S.S. Ray, Application of thin layer activation technique for monitoring corrosion of carbon steel in hydrocarbon processing environment, Appl. Radiation and Isotopes, 135, 201-206, (2018)
7. I. Kambali, H. Suryanto, Parwanto, Measuring the corrosion of aluminium by using ultra thin layer activation technique, At. Indones. 31, 35–46, (2005)
8. G. Laguzzi, L. Luvidi, N. De Cristofaro, M.F. Stroosnijder, Corrosion monitoring of different steels by thin layer activation, J. Radioanal. Nucl. Chem. 262 (2), 325–330, (2005)
9. Mf. Stroosnijder, M. Hoffmann, T. Sauvage, G. Blondiaux, L. Vincent, Wear evaluation of a cross-linked medical grade polyethylene by ultra thin layer activation compared to gravimetry, Nucl Instruments Methods Phys Res Sect B, 225, 597–602, (2005)
10. Y. Wang, Ma. Nastasi, Handbook of modern ion beam materials analysis, Warrendale, Pennsylvania: Materials Research Society, (2009)
11. M. Scherge, K. Pohlmann, A. Gerve, Wear measurement using radionuclide technique (RNT), Wear, 254, 801–817, (2003)
12. International Atomic Energy Agency, Radiation Technology for Cleaner Products and Processes, IAEA-TECDOC-1786, IAEA, Vienna, (2016)

Pitting factor in use of galvanostatic pulse method for measuring the corrosion rate of reinforcement in concrete

Davor Grandić[1], Ivana Štimac Grandić[1]
Faculty of Civil Engineering, University of Rijeka, Croatia [1]

E-mail: davor.grandic@gradri.uniri.hr

Abstract: *Corrosion of steel reinforcement in concrete is the most common cause of deterioration of reinforced concrete structures which ultimately leads to structural failure. Maintenance and repair of concrete structures exposed to corrosion of reinforcement causes high costs worldwide. The simplest and at the same time practical mathematical model of corrosion degradation of reinforced concrete structures is to determine the remaining diameter of reinforcing bars based on the depth of corrosion penetration. The real depth of corrosion penetration differs from the corrosion depth that can be determined from the measured corrosion rates. To establish a relationship between the corrosion depths determined from measured corrosion rates and real depths of corrosion penetration, it is necessary to determine the so-called pitting factor. This paper will present the values of pitting factors for hot rolled and cold worked steel reinforcement bars embedded in concrete beam and slab specimens, using the galvanostatic pulse method and GalvaPulse measuring equipment.*

Keywords: STEEL RENFORCEMENT CORROSION, CORROSION RATE, PITTING FACTOR

1. Introduction

Corrosion of reinforcement in concrete is an electrochemical process that occurs when the following conditions are met: difference in potential on the steel surface, electrolytic bonding of steel surface parts with different potentials, active state on anode parts where reinforcement is damaged and sufficient oxygen binding electrons released on cathode parts steel fittings [1]. The first condition is mostly satisfied due to the inhomogeneous structure of steel and inhomogeneous contact of concrete and steel in reinforced concrete. Concrete usually has enough free and absorption-bound water to serve as an electrolyte. However, under normal conditions, steel reinforcement in concrete does not corrode. The reason for this is the presence of a passive (protective) layer of iron oxide on the surface of the reinforcement. The passive layer can be destroyed by carbonation of concrete and/or due to the presence of chloride ions in the reinforcement environment. The mechanism of ion penetration into concrete is most often described by the second Fick's law of diffusion, but there can be other mechanisms and their combination with diffusion, i.e. capillary absorption and flow of fluid under pressure through the porous structure of concrete [2].

Chlorides locally destroy the passive layer around the reinforcement bars, causing pitting or localized corrosion [3]. It follows from the above that the process of corrosion of reinforcement in concrete is influenced by several factors that are randomly distributed, in space and in time.

The most important parameter used in mathematical models of deterioration of reinforced concrete structures in a corrosive environment is the corrosion rate [4-6]. The corrosion rate depends on changes in humidity and temperature during the year and on the arrangement and width of cracks in the concrete.

The influence of pitting corrosion induced by chlorides on the reduction of reinforcement diameter is usually considered by introducing the so-called "pitting factor" which is defined as the ratio of real reduction of corroded reinforcement diameter and average depth of corrosion penetration into reinforcement [4, 5, 7]. However, the "pitting factor" defined in this way can, depending on the degree of corrosion and other circumstances such as the cracking of concrete, vary within wide limits [4, 5, 7].

The average corrosion penetration depth can be determined from the mass of the corroded bar [7] or calculated from the results of corrosion rate measurements [4, 5, 6, 8].

The measured corrosion rates refer to the part of the reinforcing bar covered by the measuring range of the sensor [9], while the data of the corrosion between the discretely arranged measuring points are not known. The magnitudes of the measured corrosion rates are significantly influenced by the applied corrosion rate measurement technique [10]. Two commonly used techniques in portable corrosion measurement equipment are the linear polarization method (LPR technique) and the galvanostatic pulse method (GPM technique) [10]. It was found, however, that regardless of the applied measuring technique the magnitude of measured corrosion rates in the observed period on the same structure differ mainly in intensity but not qualitatively, i.e. corrosion rates differ for scalar throughout the measurement period [10].

In this paper, the values of pitting factors for hot rolled and cold worked reinforcement embedded in concrete samples of beams and slabs are determined using the galvanostatic pulse method and GalvaPulse measuring equipment.

2. Relationship between pitting factor and residual cross-sectional area of corroded reinforcing bars

The remaining cross-sectional area of corroded reinforcement is defined differently depending on whether it is homogeneous or localized, i.e. pitting corrosion. Homogeneous corrosion occurs under conditions of carbonation of concrete, while chloride ions cause localized corrosion known as pitting corrosion which causes a significant reduction in reinforcement cross section [4, 5].

In the case of homogeneous corrosion, corrosion penetrates uniformly into the reinforcement over the entire surface of the bars, so the average depth of corrosion penetration in the measuring range of the sensor can be calculated from the results of measuring the corrosion rate according to [11, 12]:

$$P_{\mathrm{i,corr}} = 11,6 \cdot \int_{t_{\mathrm{ini}}}^{\tau} i_{\mathrm{corr}} \mathrm{d}t \,, \tag{1}$$

where $P_{i,\mathrm{corr}}$ is the mean corrosion depth in microns, i_{corr} is the corrosion rate in $\mu A/cm^2$ measured at time t, $(\tau - t_{\mathrm{ini}})$ is the duration of corrosion in years, t_{ini} is the time of corrosion initiation and τ is time in which P_{corr} is calculated.

According to the conservative model [4, 5], the residual cross-sectional area of the reinforcement can be estimated on the basis of the residual diameter of the corroded reinforcement ϕ, which is determined by the following expression:

$$\phi = \phi_0 - \alpha P_{\mathrm{i,corr}} \,, \tag{2}$$

where α is the so-called pitting factor which takes into account the type of corrosion of the reinforcement. In the case of homogeneous corrosion, the value of α is 2, and in the case of localized corrosion, the coefficient α can reach the value of 10 when the corrosion rate is measured by the linear polarization method [4, 5, 7] (Fig. 1).

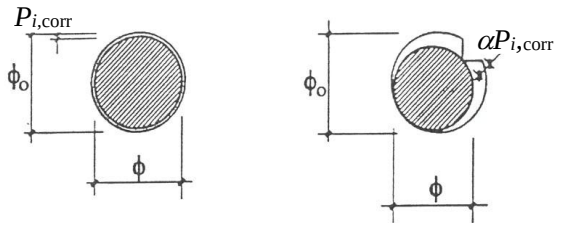


Fig. 1 *Cross-section of corroded reinforcement (left: homogenous corrosion, right: pitting corrosion) [4, 5]*

Fig. 1 shows that the pitting factor α in Equation 2 can be defined as the ratio of the maximum depth of reinforcement corrosion at the position of local damage (i.e. "pit") and the mean value of the depth of corrosion.

The cross-sectional area of the corroded reinforcement determined from the remaining bar diameter obtained according to Equation 2 is a conservative value, as can be seen in Fig. 1 (shaded area on the cross-section of the bar, left). For a more realistic determination of the remaining cross-sectional area of corroded reinforcement, based on the depth of the "pit" it is necessary to assume the shape of the pit. In the articles [13–15] and in LIFECON-Service Life Models [16], a circular shape of "pits" in cross-section of bars is assumed (Fig. 2).

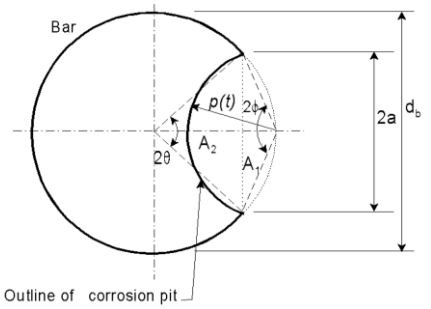


Fig. 2 *The assumed circular shape of the pit - pit depth is denoted by p(t) [16]*

However, the simplified assumption of the residual cross-sectional area A_{res} of corroded reinforcement cannot cover all cases of localized corrosion along reinforcing bars. For example, the form of localized corrosion (pitting) can manifest in different shapes, dimensions and depths of reinforcement damage [17-19]. Nevertheless, we believe that the value of the pitting factor related to the corrosion rate measurement technique is useful for the condition assessment of reinforced concrete structures exposed to reinforcement corrosion.

3. Experimental Program

A comprehensive experimental research was conducted, where data about advancement of chloride corrosion of reinforcement, and damaging effects of corrosion on reinforced concrete elements simultaneously exposed to sustained load was collected [11, 12]. The beam specimens had a cross-section of 8×12 cm and length of 200 cm. Slab specimens had a cross-section 50×8 cm, and length of 200 cm. The concrete cover to the reinforcement was 1,0 cm (Fig. 1 and Fig. 2).

Reinforcing bars of 6 mm nominal diameter were of cold worked ribbed reinforcing steel, while the ones of nominal diameter of 8 mm were of hot rolled ribbed reinforcing steel.

Material properties were determined by testing. Mean values of tested specimens are hereby specified: yielding strength of 589 MPa, tensile strength of 684 MPa and strain at maximum force of 6,38% were determined for hot rolled reinforcing steel while yielding strength of 573 MPa, tensile strength of 607 MPa and strain at maximum force of 2,13% were determined for cold worked reinforcing steel. Compressive strength of 28 day-old concrete was tested on concrete cubes with edge length of 150 mm, and mean value of testing results was 35,2 MPa.

Testing determined the mean value of the coefficient of capillary absorption of concrete is 0,62 $kgm^{-2}h^2$ and mean value of specific coefficient of gas permeability is $1{,}353 \cdot 10^{-13} cm^2$. Resistance to penetration of chloride ions is evaluated [13] over the quantity of electricity which passed through the rolled specimens of nominal diameter of 102 mm and nominal high of 51 mm. Mean quantity of passing electricity through the specimens was 1249 coulombs. Results of testing show that the specimens of beams and slabs were composed of concrete of mean quality according to transport-related properties [20, 21].

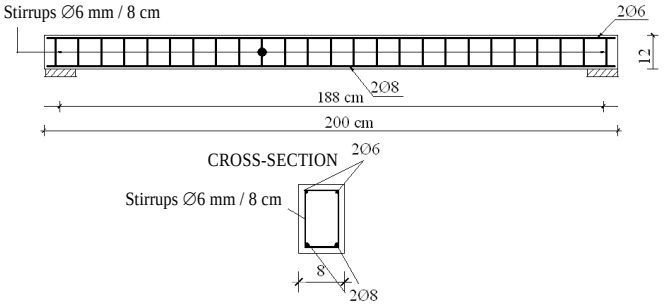


Fig. 3 *Beam specimen [11, 12]*

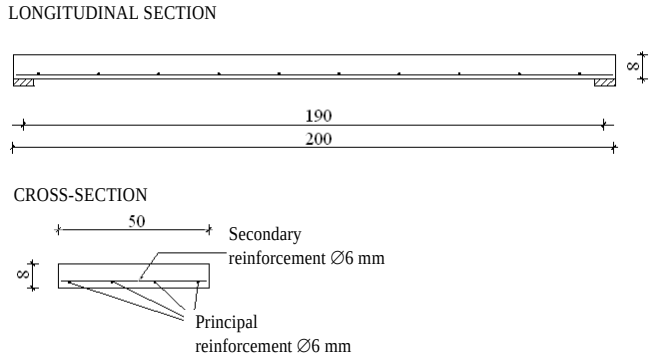


Fig. 4 *Slab specimen [11, 12]*

Three levels of reinforcement corrosion were foreseen in the experimental programme. First level of reinforcement corrosion is determined as $P_{i,corr} \approx 0{,}05$ mm, second level as 0,1 mm $\leq P_{i,corr} <$ 0,2 mm and third level as $P_{i,corr} > 0{,}2$ mm.

For each level of corrosion, a series of four specimens of reinforced concrete beams and slabs were foreseen (a total of 16 beams and 16 slabs).

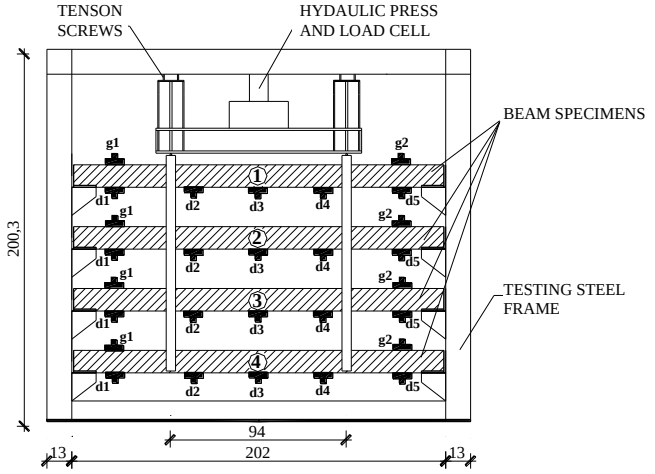
Initiation and acceleration of reinforcement corrosion in reinforced concrete beams and slabs was conducted in environmental chamber by repeating the 3-day cycles of wetting specimens by spraying with salt water and drying them [12]. The concentration of sodium-chloride (NaCl) in salt water used to spray specimens was 3,8% in relative to the water mass. The total duration of corrosion process in environmental chamber last for 383 days (109 cycles).

Specimens of beams and slabs were exposed to constant sustained loading in steel frames during the exposure to reinforcement corrosion. Sustained loading of specimens caused cracks in concrete with average width of 0,1 mm.

Periodically, the reinforcement corrosion parameters (corrosion rate, half-cell potential and electrical resistance), were measured on specimens of reinforced concrete beams and slabs. After reaching each degree of reinforcement corrosion - one specimen of beams and slabs from the series were destroyed, the reinforcement was removed to conduct a detailed examination, measuring and testing of corroded reinforcement. Other specimens were tested by loading to failure to establish the bearing capacity of beams and slabs subjected to reinforcement corrosion (not in focus of this paper).

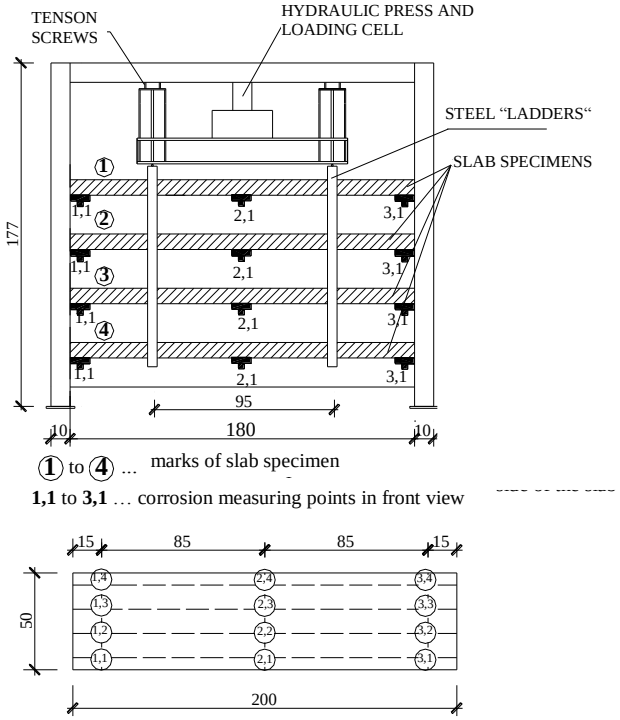
4. Measuring of Reinforcement Corrosion Parameters

During the exposure of beam and slab specimens to reinforcement corrosion a total of 18 phases of measurements of corrosion parameters were conducted. GalvaPulse^{TM} device based on galvanostatic impulse method was used for the measurements [11, 12].



① to ④ ... marks of beam specimen
g1, g2 … corrosion measuring points on the top side of the beams
d1 to d5 … corrosion measuring points on the bottom side of the beams

Fig. 3 *Beam specimens in the testing frame and corrosion measurement points [11, 12]*



① to ④ ... marks of slab specimen
1,1 to **3,1** … corrosion measuring points in front view
1,1 to **3,4**… corrosion measuring points on the bottom side of the slab

Fig. 4 *Slab specimens in the testing frame and corrosion measurement points [11, 12]*

The corrosion parameters were measured at two points on the upper surface and at five points on the bottom surface of each beam specimen. On the slab specimen, corrosion was measured at 12 points on the bottom surface of the slabs. The position of beam and slab specimens in the testing frames and the points of corrosion measurements are shown in Fig. 3 and Fig. 4.

The measured values of corrosion parameters (corrosion rate, half-cell potential and electrical resistance) are presented in detail in paper [12].

5. Determination of the pitting factor

Loss of mass and depth of corrosion penetration into the reinforcement were determined on corroded reinforcing bars extracted from concrete specimens, after each reinforcement corrosion level reached (a total of three corrosion levels, as mentioned previously). The depth of corrosion at the pit position P_{pit} was measured with a point micrometer at the position of the greatest corrosion damage of the corroded reinforcement sample. Corrosion depths $P_{i,corr}$ based on GPM technique corrosion measurements were determined using expression (1) and numerical integration. The length of the measuring range of the sensor (GalvaPulse) is 70 mm. Pitting factor α is determined by the following expression:

$$\alpha = \frac{P_{pit}}{P_{i,corr}} \tag{3}$$

5.1 Hot rolled longitudinal beam reinforcement

From the specimens of beams that reach the first, second and third level of corrosion, five reinforcing bar samples were taken, the order of which (from 1 to 5) corresponds to the position of corrosion measuring points along the beams (Fig. 3).

The labelling of an individual beam specimen consists of mark GI, GII or GIII which denote series of beams in which the different level of reinforcement corrosion was reached (levels I, II and III) and label 1 to 4 representing the position of the beam specimen in the test frame (Fig. 3).

Tables 1 to 3 show the mass losses, the corrosion depth at the pit position P_{pit} and the corrosion depths determined from the corrosion measurement results $P_{i,corr}$. The following notations are additionally used in the tables:
L - the length of the corroded reinforcement sample (mm)
M - mass of corroded reinforcement sample (g)
m - length mass of corroded reinforcement (g/mm), $m = M/L$
m_0 - initial length mass of uncorroded reinforcement (g/mm)
Δm - loss of length mass determined by reinforcement weighing (g/mm), $\Delta m = m_0 - m$.

The initial length mass of uncorroded reinforcement m_0 is 0,4264 g/mm for nominal diameter of bars of 8 mm,

Table 1*: Weight loss and pitting factor, beam specimen GI-4*

Bar sample	L [mm]	M [g]	m [g/mm]	Δm [g/mm]	$\Delta m/m_0$ [%]	P_{pit} [mm]	$P_{i,corr}$ [mm]	a
1	395,49	162,2300	0,4102	0,0162	3,80	0,31	0,037	8,53
2	391,20	160,1964	0,4095	0,0169	3,96	0,28	0,065	4,35
3	384,50	158,1833	0,4114	0,0150	3,52	0,30	0,055	5,48
4	395,04	161,8479	0,4097	0,0167	3,92	0,24	0,055	4,41
5	389,40	159,2257	0,4089	0,0175	4,10	0,22	0,044	5,10

Table 2*: Weight loss and pitting factor, beam specimen GII-3*

Bar sample	L [mm]	M [g]	m [g/mm]	Δm [g/mm]	$\Delta m/m_0$ [%]	P_{pit} [mm]	$P_{i,corr}$ [mm]	a
1	391,83	154,3844	0,3940	0,0324	7,60	0,35	0,113	3,12
2	390,31	153,6916	0,3938	0,0326	7,65	0,37	0,155	2,41
3	390,14	153,4614	0,3933	0,0331	7,75	0,37	0,197	1,90
4	394,71	155,4118	0,3937	0,0327	7,66	0,33	0,205	1,62
5	395,30	156,2034	0,3952	0,0312	7,33	0,34	0,112	3,08

Table 3*: Weight loss and pitting factor, beam specimen GIII-3*

Bar sample	L [mm]	M [g]	m [g/mm]	Δm [g/mm]	$\Delta m/m_0$ [%]	P_{pit} [mm]	$P_{i,corr}$ [mm]	a
1	365,00	144,4748	0,3958	0,0306	7,17	0,50	0,147	3,42
2	409,85	161,2990	0,3936	0,0328	7,70	0,67	0,246	2,74
3	365,37	143,4460	0,3926	0,0338	7,93	0,61	0,245	2,50
4	415,45	163,4729	0,3935	0,0329	7,72	0,59	0,289	2,05
5	415,51	164,1946	0,3952	0,0312	7,33	0,44	0,159	2,79

The correlation between corrosion depth $P_{i,corr}$ and pitting factor α for corroded hot rolled reinforcement in beam specimens can be established as it can be seen in Fig. 5.

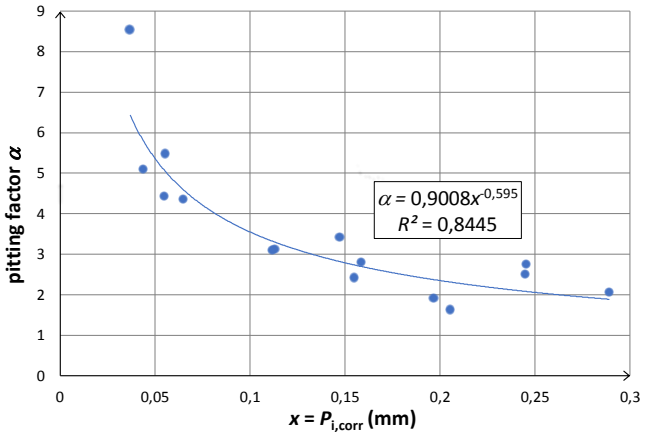


Fig. 5 *Relation between corrosion depth $P_{i,corr}$ and pitting factor α for hot rolled beam reinforcement*

In the case of beam specimen reinforced with hot rolled steel bars, the pitting factor decreases with the progression of reinforcement corrosion. The highest value of pitting factor of 8,53 is in case of low corrosion of the reinforcement. With further progress of reinforcement corrosion, the pitting factor decreases rapidly, and its value is approximately 2 for significant reinforcement corrosion.

5.2 Cold worked longitudinal slab reinforcement

From the specimens of slab that have reached the first, second and third levels of corrosion, three reinforcing bar samples are taken out, the order of which (from 1 to 3) corresponds to the position of corrosion measuring points along the slab specimen (Fig. 4). Marks PI, PII, PIII denote series of slabs in which the different level of reinforcement corrosion were reached (levels I, II and III). The labelling of an individual slab specimen consists of the mark PI, PII or PIII and numbers 1 to 4 representing the position of the specimen in the test frame (Fig. 4).

Tables 4 to 6 show the mass losses, the corrosion depth at the pit position P_{pit} and the corrosion depths determined from the corrosion measurement results $P_{i,corr}$. The initial length mass of uncorroded reinforcement m_0 is 0,2082 g/mm for nominal diameter of bars of 6 mm,

Table 4*: Weight loss and pitting factor, slab specimen PI-2*

Bar sample	L [mm]	M [g]	m [g/mm]	Δm [g/mm]	$\Delta m/m_0$ [%]	P_{pit} [mm]	$P_{i,corr}$ [mm]	a
1	396,57	82,2411	0,20738	0,00082	0,393	0,40	0,044	9,13
2	494,91	102,6230	0,20736	0,00084	0,405	0,41	0,058	7,04
3	342,52	69,8981	0,20407	0,00413	1,984	0,05	0,037	1,35

Table 4*: Weight loss and pitting factor, slab specimen PII-3*

Bar sample	L [mm]	M [g]	m [g/mm]	Δm [g/mm]	$\Delta m/m_0$ [%]	P_{pit} [mm]	$P_{i,corr}$ [mm]	a
1	444,99	91,5336	0,20570	0,00250	1,202	0,99	0,079	12,48
2	356,35	72,3063	0,20291	0,00529	2,542	1,72	0,148	11,61
3	356,30	73,6161	0,20661	0,00159	0,762	0,00	0,068	0,00

Table 4*: Weight loss and pitting factor, slab specimen PIII-1*

Bar sample	L [mm]	M [g]	m [g/mm]	Δm [g/mm]	$\Delta m/m_0$ [%]	P_{pit} [mm]	$P_{i,corr}$ [mm]	a
1	361,23	74,3715	0,20588	0,00232	1,112	0,29	0,153	1,90
2	354,56	71,6718	0,20214	0,00606	2,909	0,77	0,272	2,83
3	450,87	90,9239	0,20166	0,00654	3,140	0,27	0,136	1,99

As it is shown in Figure 6, there is no corelation between corrosion depth $P_{i,corr}$ and pitting factor α for corroded cold worked reinforcement of slabs. The values of pitting factor vary from 0 to 12,48. Roughly and on the safe side it can be accepted for $P_{i,corr} \leq$ 0,15 mm the pitting factor is α = 12, and for $P_{i,corr}$ > 0,15 mm the pitting factor is α = 3.

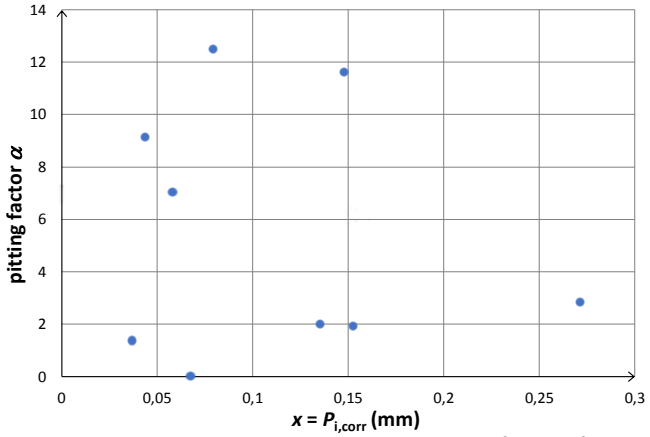


Fig. 6 *Relation between corrosion depth $P_{i,corr}$ and pitting factor α for cold worked slab reinforcement*

5. Conclusion

This paper presents the values of pitting factors for hot rolled and cold worked steel reinforcement bars embedded in concrete beam and slab specimens exposed to accelerated corrosion of reinforcement in the salt environmental chamber using the galvanostatic pulse method and GalvaPulse measuring equipment.

The corrosion depths are firstly calculated from the measured values of reinforcement corrosion rates. The corrosion depths determined form corrosion rate measurement are the mean values of the corrosion depths within the measuring range of the GalvaPulse measuring device. Since chloride corrosion of reinforcement by its nature is localised corrosion („pitting“), the actual corrosion depths at the pit location differ from the corrosion depths determined based on corrosion rate measurements. Therefore, measurements of corrosion depths at the pit location on reinforcing bars extracted from corroded samples of beams and slabs were performed. The relation between measured corrosion depth at the pit position and calculated corrosion depth using measured values of reinforcement corrosion rates is defined as pitting factor.The pitting factor should be determined for each measuring technique and measuring device.

The results presented in this paper, in the case of applying the galvanostasis pulse method using the GalvaPulse measuring device, show the following:

- The correlation between the corrosion depth calculated from the measured corrosion rates and the pitting factor can be established for hot rolled reinforcement in beam specimens.
- The pitting factor for hot rolled reinforcement in beams decreases with the progress of corrosion, i.e. it decreases with increasing of reinforcement corrosion.
- For cold worked reinforcement in slab specimens the correlation between the corrosion depth calculated from the measured corrosion rates and the pitting factor cannot be established.
- It is proposed to use two values of the pitting factor for cold worked reinforcement in slabs depending on the value of the corrosion depth determined based on the corrosion rate measurement.

6. References

[1] Luca Bertolini, Bernhard Elsener, Pietro Pedeferri, Elena Redaelli, Rob B. Polder: Corrosion of Steel in Concrete: Prevention, Diagnosis, Repair, 2nd Edition, Wiley-VCH, 2014.
[2] Li, C. Q.; Zheng, J. J.; Shao, L.: New Solution for Prediction of Chloride Ingress in Reinforced Concrete Flexural Member, ACI Materials Journal, 100(2003) 4, 319-325.
[3] John P. Broomfield: Corrosion of Steel in Concrete; Understanding, investigation and repair, 2nd edition, Taylor & Francis, USA and Canada, 2007.

[4] Rodríguez, J.; Ortega, L. M.; Aragoncillo, J.; Izquieredo, D.; Andrade, C.: Structural assessment methodology for residual life calculation of concrete structures affected by reinforcement corrosion, International RILEM Workshop on Life Prediction and Aging Management of Concrete Structures, Canes, France, 2000, 97-112.
[5] CONTECVET, A validated users manual for assessing the residual life of concrete structures – Manual for assessing corrosion-affected concrete structures, Instituto Eduardo Toroja, EC innovation programme IN30902I, Madrid, 2000.
[6] Mangat, S.P.; Elgarf, M.S.: Flexural Strength of Concrete Beams with Corroding Reinforcement, ACI Structural Journal 96 (1999) 1, 149-159.
[7] González, J.A.; Andrade, C.; Alonso, C.; Feliu, S.: Comparasion of rates of general corrosion and maximum pitting penetration on concrete embedded steel reinforcement, Cement and Concrete Research 25 (1995) 2, 257-264.
[8] Klinghoffer, O.; Frølund, T.: Rebar Corrosion Rate Measurements for Service Life Estimates, ACI Fall Convention 2000, Toronto, Canada, Committee 365 "Practical Application of Service Life Models".
[9] Brite-Euram III "Smart Structures", Contract No. BRPR-CT98-0751: Integrated Monitoring Systems for Durability Assessment of Concrete Structures, Project Report, September 2002.
[10] Poursaee, A.: An Analysis of the Factors Influencing Electrochemical Measurements of the Condition of Reinforcing Steel in Concrete Structures, Ph.D. thesis in Mechanical Engineering, University of Waterloo, Ontario, Canada, 2007.
[11] Grandić, D.: Calculation procedures for evaluating remaining load bearing capacity and serviceability of corroded reinforced concrete structures, Doctoral Thesis, Faculty of Civil Engineering, University of Zagreb, Croatia, 2008. (in Croatian)
[12] Grandić, D.; Bjegović, D.: "Reinforcement Corrosion Rate in Cracked Areas of RC-Members Subjected to Sustained Load", Andrade, C.; Mancini, G. (ur.), Modelling of Corroding Concrete Structures - Proceedings of the Joint fib-RILEM Workshop held in Madrid, Spain, November 2010, Heidelberg, Njemačka: Springer, 2011., str. 65-83. (ISBN: 978-94-007-0676-7)
[13] Cairns, J.; Plizari, G.A.; Du, Y.; Law, D.W.; Franzoni, C.: Mechanical Properties of Corrosion-Damaged Reinforcement, ACI Materials Journal, 102 (2005) 4, 256-264.
[14] Val, D.V.; Melchers, R.E.: Reliability of Deteriorating RC Slab Bridges, Journal of Structural Engineering, December 1997, 1638-1644.
[15] Stewart, M.G.; Al-Harthy, A.: Pitting corrosion and structural reliability of corroding RC Structures: Experimental data and probabilistic analysis, Reliability Engineering and System Safety 93 (2008), 373-382.
[16] Sascha Lay, Peter Schießl: LIFECON DELIVERABLE D 3.2 - Service Life Models, Technische Universität München, 2003.
[17] Pallson, R.; Mirza, S.M.: Mechanical response of corroded steel reinforcement of abandoned concrete bridge, ACI Structural Journal, 99 (2002) 2, 157-162.
[18] Tang, F.; Lin, Z.; Chen, G.; Yi, W.: Three-dimensional pit measurements and statistical mechanical degradation analysis of deformed steel bars subjected to accelerated corrosion, Construction and Building Materials, 70 (2014), 104-117.
[19] Apostolopoulos, C.A.; Demis, S.; Papadakis, V.G.: Chloride-induced corrosion of steel reinforcement – Mechanical performance and depth analysis, Construction and Building Materials, 38 (2013), 139-146. http://dx.doi.org/10.1016/j.conbuildmat.2012.07.087
[20] ASTM Designation: C 1202 - 91: Standard Test Method for Electrical Indication of Concrete's Ability to Resist Chloride Ion Penetration.
[21] Ukrainczyk, V.; Bjegović, D.: Materials testing in the insurance system of durability of concrete structures, Civil engineering yearbook 1995, Croatian Society of Civil Engineers, Zagreb, Croatia, 1995., pp. 209-286. (in Croatian)

The application of rapid prototyping in the studing of samples of filtering materials based on woven nets

Aliaksandr Ilyushchanka[1, 2], Iryna Charniak[2], Aliaksei Kusin [2], Vecheslav Kaptsevich[3], Ruslan Kusin[3], Nataliai Rutkovskaya[3], Dmitry Shamal[4],
State research and production powder metallurgy association[1] – Minsk, Republic of Belarus
State Scientific Institution "O.V. Roman Powder Metallurgy Institute" [2] – Minsk, Republic of Belarus
Belarusian state agriculture technical university [3] – Minsk, Republic of Belarus
"3D systems" [4] – Minsk, Republic of Belarus
E-mail: alexil@mail.belpak.by, irinacharniak@tut.by, 2312444@mail.ru, 19081877@mail.ru, info@additive.by

Abstract: *In the paper consider materials for the rapid prototyping (RP) of experimental samples of filtering materials with an orthotropic structure based on woven nets (FMWN) assembled together with test-form and with using of 3D printing. RP made it possible to reduce the labor intensity of the process, primarily by eliminating the operation of sealing samples when using a traditional test form, as well as making the test form and the samples themselves. The data obtained allowed us to conclude that the use of 3D-printing is promising in further work for the manufacture of test form for studying the properties of filtering materials.*
KEYWORDS*: FILTER MATERIALS, WOVEN MESH, 3D PRINTING, SAMPLES, RESEARCH, PROPERTIES*

1. Introduction

At this time, additive technologies have found application in various fields of the national economy, including in mechanical engineering, medicine, construction and others [1, 2]. Due to its advantages: the ability to quickly change the shape of manufactured parts, which makes it possible not only to quickly obtain prototypes, but also to make changes to the basic design in accordance with the wishes of a particular customer, high dimensional accuracy of manufactured products, the possibility of switching from mass production to mass customization (the possibility of satisfying as many individual customers as possible), the possibility of creating products with a complex shape or even impossible configuration in conventional production, significantly reduce the duration of the production cycle, the timing and cost of launching the product into production (due to the lack of need for specialized tooling), increase the material utilization rate, reduce greenhouse gas emissions by optimizing product design and reducing material losses, production mobility (the time from the moment of product design to the receipt of the finished part can be reduced from several weeks to several days) and accelerate data exchange – 3D printing is considered to be a breakthrough technology that can change industrial production in the foreseeable future [3, 4]. The achievements of computer technologies arouse interest in new methodologies and technologies for improving and accelerating the development of subjects, objects, and materials. Rapid prototyping is a promising direction in this area [5, 6].

Rapid prototyping is used for the manufacture of filter materials with an orthotropic structure based on woven meshes (FMWN) intended for scientific research.

The structure and advantages of these materials are described in [7]. The application of the method was caused by the complexity of the design, manufacture, assembly and disassembly directly in the process of determining the filtering characteristics of the samples: the main difficulty was the need to ensure the sealing of the sample on all the surfaces bordering the tooling. It should be noted that similar problems were solved by the authors [8] (Figure 1).

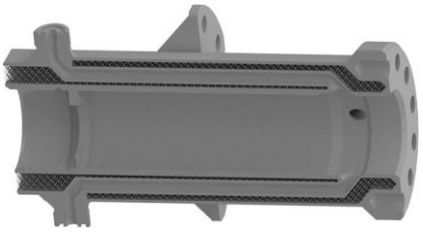


Fig. 1 *Example of the implementation of mesh structures in the design of a part*

The purpose of the work is to exchange experience in the use of rapid prototyping of filter materials with an orthotropic structure based on woven nets.

2. The results of the experiment and their discussion

3D – modeling and 3D – printing were used for the production of samples. The samples were produced on a 3D printer of the Uniz SLASH 2 model from a polymer material of the brand-the photopolymer Dentifix-3D Modeling HR. A model image of an experimental FMWN sample in the form of three projections is shown in Figure 2, a 3D model of one layer of an experimental sample made of woven mesh is shown in Figure 3. The technology of production of samples included the following stages. At the first stage, the FMWN was made with sealing along the contour at the border with the tooling (Figure 4), then the second part of the housing was made for supplying air or liquid, depending on the operation performed and connecting to the pressure gauge (Figure 5) and glued the tooling (Figure 6). The different stages of the process are shown in Figure 7, and the process of determining the size of pores is shown in Figure 8.

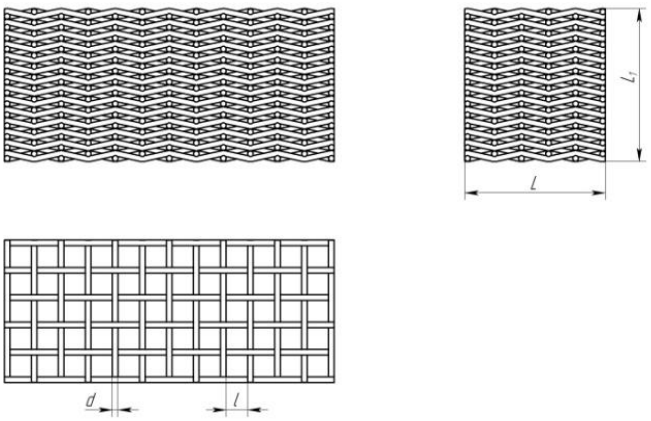


Fig. 2*. Model image of the experimental sample*

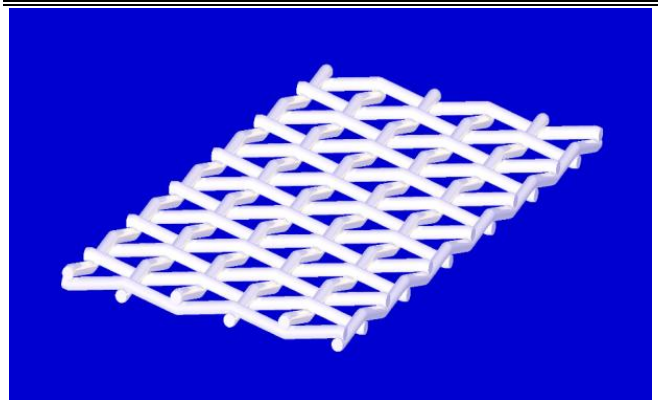


Fig. 3. *3D model of a woven mesh layer for the production of an experimental sample FMWN*

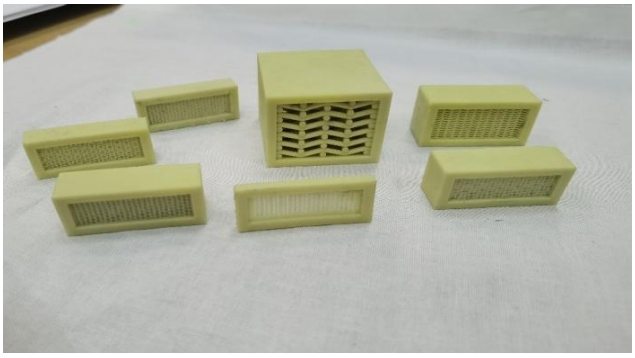


Fig. 4. *Physical appearance of samples from FMWN made with a part of the housing*

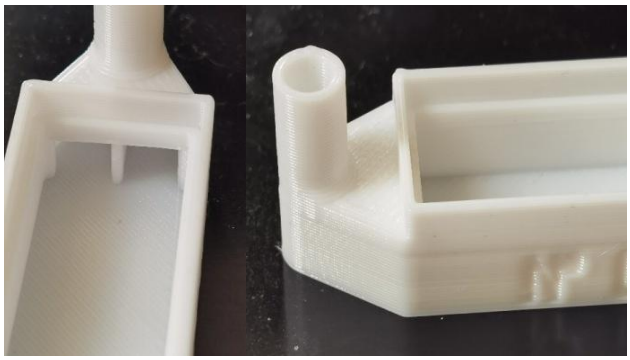


Fig. 5. *Photos of the lower part of the housing for the supply of technological media and connection to the pressure gauge*

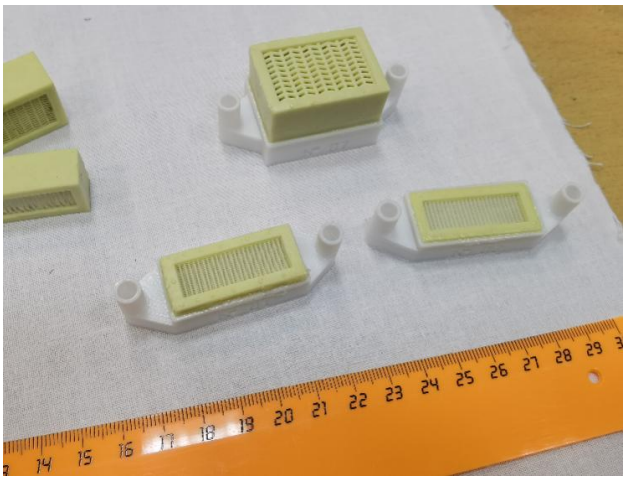


Fig. 6. *Physical appearance of the samples in the assembling*



Fig. 7. *Different stages of the sample production process*



Fig. 8. *The process of determining the size of pores*

The samples made it possible at the initial stage of research to establish the relationship of pore sizes, filtration fineness, permeability coefficient from the characteristics of woven meshes (wire diameter and cell size in light) and the thickness of the filter layer. The use of 3D modeling and 3D printing in the production of experimental samples has reduced the complexity of the process, especially in terms of sealing samples before measurements, as well as production equipment and samples themselves. In addition, the experience gained allowed us to conclude that it is promising to use the 3D printing method in the future for the production of equipment for studying the properties of filter materials

Conclusion

The materials on rapid prototyping of experimental samples of filter materials with an orthotropic structure based on woven meshes (FMWN) assembled with equipment using 3D printing are presented, which made it possible to reduce the complexity of the process, first of all, sealing the samples before measurements, as well as production the equipment and the samples themselves. The experience gained also allowed us to draw a conclusion about the prospects of using 3D printing in the future for the production of equipment for studying the properties of filter materials. The disadvantages that should be taken into account in the future (for example, by introducing correction coefficients) you can include the fact that it is impossible to take into account the influence of deformation of mesh layers on the properties of FTWN during the study

3. References

1. Apostolov, A. Review of the application of additive technologies in research in the field of chemistry and chemical engineering, Advances in chemistry and chemical Technology, Volume XXXIV. 2020. No. 6. pp. 29-34. (A. Apostolov).

2. Zlenko, M. Additive technologies in mechanical engineering, Manual for engineers, Moscow, SSC RF FSUE "NAMI", 2015, 220 p. (M. Zlenko, M. Nagaytsev, V. Dovbysh).

3. Tomashev, V. Actual problems and innovative methods of production based on the use of additive technologies, Scientific research: theory, methodology and practice, Cheboksary, CNS "Interactive Plus", 2017, Vol. 2, pp. 88-91. (V. Tomashev, T. Zaitseva, N. Oreshkina, E. Zagrebina).
4. Litunov, S. Review and analysis of additive technologies, Part 1, Omsk Scientific Bulletin, 2016, No. 1 (145), pp. 12-13. (S. Litunov, V. Slobodenyuk, D. Melnikov).
5. Dheeraj Nimawat, Using Rapid Prototyping Technology In Mehanical Scale Models, International Journal of Engineering Research and Applications (IJERA), 2012. Vol.2. Issue 2. Pp. 215-219. (Dheeraj Nimawat, Mahaveer Meghvanhi).
6. Gritskevich, E. 3D modeling technologies and digital prototyping in mechanical engineering, Forest engineering: problems and prospects of development, Krasnoyarsk, 2017, pp. 27-31. (E. Gritskevich, A. Gaibov).
7. Ilyushchanka, A. Modeling filter material with an orthonotropic structure based on woven wesh, MATEC Web of Conferences, 2020, **317**, 06001, Power transmissions 2020. (A. Ilyushchanka, I. Charniak, V. Kaptsevich, V. Korneeva, R. Kusin, I. Zakreuski, P. Chyhayeu).
8. Gorbatov, I. Determination of the possibility of creating mesh structures in their manufacture using additive technologies, Bulletin of the Concern of aerospace defense "Almaz-Antey", 2020, No. 2, pp. 74-82. (I. Gorbatov, A. Pilshchikov, Yu. Orlov, V. Antyufeev, S. Antyufeev, N. Orlova, D. Karpov).

Testing of technology for joining materials in the automotive industry

Emil Evin[1], Ján Viňáš[2], Dušan Sabadka[1]
Technical University in Košice, Slovakia[1]
Technical University in Košice, Slovakia[2]
dusan.sabadka@tuke.sk

Abstract: *Research on composite materials is nowadays developed on a global scale, because they have multipurpose applications. Composite materials are used in a wide range of industries. The most significant advantages of composite materials include strength, stiffness, low fibre density (e.g. carbon fibre or glass fibre), the ability to make them into any shape required for the application. The paper deals with the possibilities of joining composite materials with metallic materials. The experimental part includes tests of the strength of the chosen type of adhesive and comparison of the individual results obtained by the experiment.*
Keywords*: COMPOSITE MATERIAL, ADHESIVES, SHEAR STRENGTH, ADHESIVES JOINT*

1. Introduction

In the design of utility machines nowadays, we try to achieve the most acceptable ratio between the total weight of the machine and its overall performance and utility characteristics. This is also the reason why alloy and metal components are gradually being replaced by composite materials in such a way that their mechanical properties are either maintained or even exceeded at several times less weight. Other manufacturing efficiencies now include the search for new technological options for joining composite materials. These include riveting, ultrasonic welding, but above all bonding.

Bonding is currently the most preferred method of joining composite materials. When joining composite materials with adhesives, the selection of the correct and appropriate type of adhesive for the stressed joint is a very important and essential aspect. Shock absorption and sound reduction are also among the preferred and important properties of adhesives.

2. Theoretical backround

Composite materials are heterogeneous materials composed of two or more phases that are different in their properties. These are mechanical, physical and chemical properties. Many types of composites are known, the most used are metal-metal, metal-ceramic, polymer-ceramic, polymer-polymer, ceramic-ceramic combinations. Among the most widespread composites in the industry worldwide are composites based on organic resins, which are reinforced with different types of inorganic or ceramic fibres. The most significant advantage of composite materials with organic matrices is the synergistic combination of the lightweight and conformable formability of the unreinforced resin with the stiffness and strength of the reinforcing fibres. [4]

In contrast to other joining technologies, such as welding, bonding does not affect the material to be joined. Due to the fact that each surface of the material to be bonded has specific properties (water absorption, gas absorption, surface texture,...) there is no universal adhesive that can be used for all materials. It is therefore necessary to choose the appropriate adhesive according to the type of material to be bonded, in order to create a high quality, strong and prescribed bond. [1, 3]

In designing the joint structure, care must be taken to ensure that the bonded joint is modified to minimize blunting and bending stresses, as most bonded joints are susceptible to such stresses. With these stresses, the force is concentrated only at certain locations in the bonded joint, resulting in local concentration of forces. This can cause degeneration of the joint and subsequent damage.

The principle of the shear strength test is to determine the shear stress of a simple interlaced joint between specified adherends. These are subjected to a tensile loading force F. The result of the test is the force Fmax which is required to break the joint. The test body is clamped in jaws according to EN 1465, which are symmetrical to each other. The test itself is carried out by loading the specimen at a constant speed with a force that is in the plane of the bonded joint until the specimen breaks or is plastically deformed. The overall dimensions and shape of the individual sample follow STN EN 1465 and are shown in Fig.1 and Fig.2. The shear strength is generally given in MPa. [6]

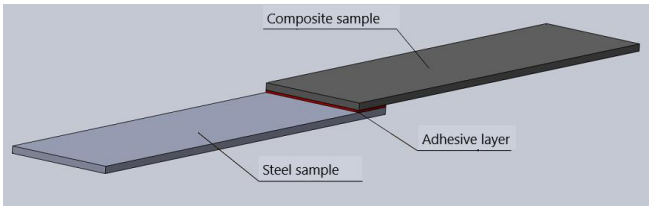


Fig.1*: Shape of the sample*

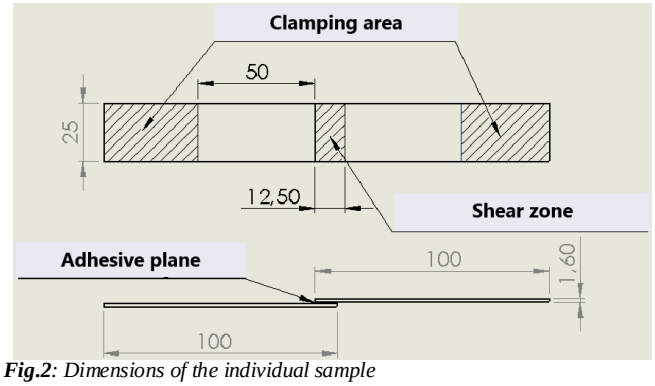


Fig.2*: Dimensions of the individual sample*

Procedure of manufacturing a bonded joint

It is important to follow the prescribed sequence of basic steps when making a bonded joint. These procedures vary depending on the properties of the adhesive and are applied according to the adhesive technical data sheet recommended by the manufacturer. The basic manufacturing procedure has 4 stages. [3, 7]

- Preparation of the adherend (material to be bonded) - surface treatment of materials - surface leveling, removal of dirt and degreasing of the surface, increasing the adhesive properties of the surface and also moisture treatment of materials with absorbent surfaces.

- Adhesive preparation

- Application of the adhesive - a continuous film of adhesive is applied to the cleaned and degreased surface of the material to be bonded. In practice, adhesives with double-sided application are more often used, because their use results in a more uniform and homogeneous film on both surfaces of the materials to be bonded. One-sided application of the adhesive is mainly used for economic reasons or in cases where two-sided application is technologically difficult.

- Installation of bonded joints - the bonded parts are fixed to each other and the prescribed pressure must be maintained.

The thickness of the adhesive layer applied is an important factor that affects the final strength of the bonded joint. If too thick a layer of adhesive is applied to the surface, the joint has little strength (Fig.3). Conversely, if a thin layer of adhesive is applied to the surface, then the joint is susceptible to dynamic stresses and is subject to rapid fatigue. [2,7]

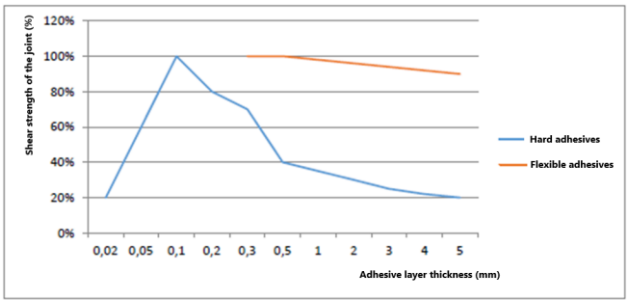


***Fig.3**: Dependence of bonded joint strength on adhesive thickness [2]*

Types of fractures of bonded joints

In all destructive tests, not only the resulting strength of the bonded joint is evaluated, but also the type of failure of the joint [2, 3, 10]. This fracture is a decisive factor in the selection of a suitable adhesive.

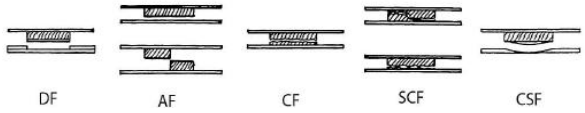


***Fig.4**: Basic types of failure of bonded joints: AF - adhesive failure, CF - cohesive failure, CSF - failure of one of the adherends, SCF - cohesive failure at the substrate boundary, DF - delamination of the substrate [8]*

3. Experimental part

The aim of the experiment was to select several types of metallic materials most used in automotive manufacturing and then bond them together with a carbon fibre composite material. Subsequently, the fabricated specimens were tested for static axial force transfer using a shear strength test. For the experimental tests, the materials most used in the automotive industry, namely stainless steel, aluminium, galvanised steel sheet and steel plate, were selected and then bonded to the composite sample. After manufacturing of the samples, the surfaces of each sample were subsequently treated. The untreated surface, the surface treated with sandpaper and the surface with notches were chosen for comparison.

Stainless steel samples

Cold rolled stainless steel sheet according to STN EN ISO 9446-2 was chosen for the production of the stainless-steel samples and is made of steel grade 1,4301+2R according to STN EN 10088-2. The thickness of the material is 1,6 mm.

Aluminium samples

The other samples were of cold rolled aluminium sheet with the designation EN AW 1050A. From this semi-finished material we produced samples with dimensions 100x25 mm as prescribed by STN EN 1465.

Galvanised sheet

Galvanised sheet is another material that was used to produce the samples. We used a 1250x2500mm sheet metal plate to produce the samples. This type of material is most commonly used for the exterior parts of car bodies, due to the fact that only corrosion of the zinc layer occurs.

Structural steel

The last type of material used is steel. Its use is common for structural frames and fixed parts of the car.

Composite steel

The composite material chosen for the experimental tests was designated CFRP, which means it is a composite with an epoxy matrix and carbon fibre. Composite samples were produced in the laboratory of the Department of Automotive Production, Faculty of Mechanical Engineering, Technical University in Košice. In this laboratory suitable conditions for the production of samples are provided, as well as ambient temperature and air humidity.

The procedure for the preparation of individual specimens consisted in cutting the carbon fibre into sheets with dimensions 600x350 mm so that the necessary number of specimens could be produced from a given sheet - for the production of 12 pieces of composite specimens with a number of reinforcements of 6, in order to achieve a total thickness of the specimen of 1.6 mm, which is prescribed by the standard STN EN 1465. The matrix was a 100:20 mixture of Epoxy Resin 285 (MGS) and Hardener 287 (MGS). The test samples were produced by hand lamination technology with subsequent air extraction from the mould. The curing time of the hand laminated sample was 24 hours. After the selected curing time, the product was removed from the mould and then the composite plate was placed in a milling machine, which was used to mill the required 100x25 mm samples

Epoxy resin was used as the adhesive, which was applied using a composite rod. The necessary thickness of the adhesive was ensured by means of demarcation wires. The thickness of the applied adhesive layer was set at 1 mm. Subsequently, all samples were labelled according to Table 1.

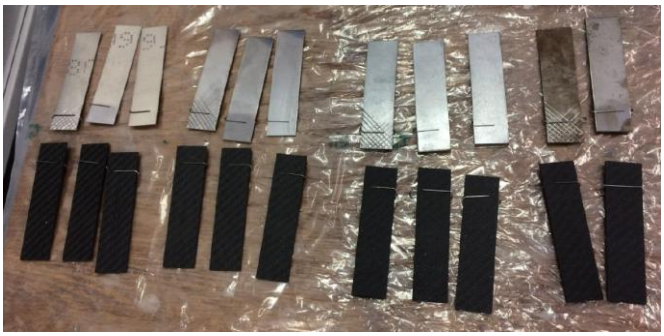


***Fig.5**: Samples prepared for bonding*

After the application of the adhesive, the joint was fixed at the overwritten overlap distance. A time limit of 48 hours was set for the adhesive to dry.

***Table 1**: Marking of sample composition*

Sample designation	Sample composition
H1	Composite + aluminum untreated sample
H2	Composite + brushed aluminum sample
H3	Composite + grooved aluminum sample
O1	Composite + untreated structural steel sample
O2	Composite + brushed structural steel sample
O3	Composite + grooved structural steel sample
N1	Composite + untreated stainless steel sample
N2	Composite + brushed stainless steel sample
N3	Composite + grooved stainless steel sample
P1	Composite + untreated galvanized sheet metal sample
P2	Composite + brushed galvanized sheet metal sample
P3	Composite + grooved galvanized sheet metal sample

Course and evaluation of the experiment

A TIRA test machine TIRA test 2300 was used to perform the shear strength test. All shear tests of bonded joints were carried out on this machine by axial static tension. The specimens were

clamped in the jaws of the testing machine at the locations previously marked and prescribed by STN EN 1465.

During the tensile shear test, the maximum F_{MAX} force transmitted through the adhesive surface was observed for each specimen. Subsequently, using this force, the maximum contracted shear stress τ_i of the bonded joint was calculated. The basis for all calculations and results was STN EN 1465. Table 3 shows the results.

***Table 2**: The conditions of the experiment*

Temperature in the laboratory at the beginning of the measurement	20,5°C
Laboratory temperature at the end of the measurement	20,8°C
Relative humidity in the laboratory	54%
Test machine jaw feed speed	10mm.min^{-1}
Maximum loading force	100 kN

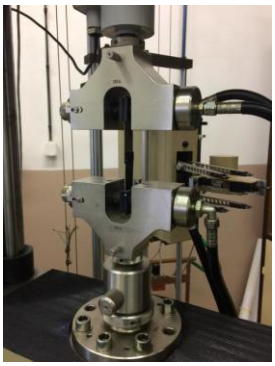


***Fig.6**: Clamping the sample into the test machine TIRA test 2300*

Sample calculation of the strength of the bonded joint of sample N1:

Given: panel width: $b_0 = 25$ mm

Overlay length: $l_0 = 12.5$ mm

Test result: $F_{N1\,MAX} = 1600$ N

$$\tau_{N1} = \frac{F_{N1\,MAX}}{S_0} = \frac{1600\ \text{N}}{25\ mm.12{,}5\ mm} = 5{,}12\ MPa$$

***Table 3**: Measurement results*

Samples	b_0 [mm]	l_0 [mm]	S_0 [mm^2]	$F_{i\,MAX}$ [N]	τ_i [MPa]
H 1	25,00	12,50	312,5	1 600,001	5,120002
H 2	25,00	12,50	312,5	2 985,243	9,552776
H 3	25,00	12,50	312,5	2 691,830	8,613857
O 1	25,00	12,50	312,5	3 354,887	10,73564
O 2	25,00	12,50	312,5	4 152,937	13,28941
O 3	25,00	12,50	312,5	4 445,952	14,22705
N 1	25,00	12,50	312,5	3 511,320	11,23622
N 2	25,00	12,50	312,5	5 022,454	16,07185
N 3	25,00	12,50	312,5	3 711,428	11,87657
P 1	25,00	12,50	312,5	3 539,113	11,32516
P 2	25,00	12,50	312,5	4 896,592	15,66909
P 3	25,00	12,50	312,5	5 842,738	18,69676

Table 3 shows the results of the experimental test. The values of the maximum force $F_{i\,MAX}$ are obtained by experiment, from which the shear stress τ_i was then calculated using the model calculation. Subsequently, these values were entered as input data into the graph in Fig.7. In the graph it is possible to compare the individual forces that the bonded joint withstood. From the overall results, the aluminium composite specimens came out the weakest, as in all cases the total force $F_{i\,MAX}$ was the lowest.

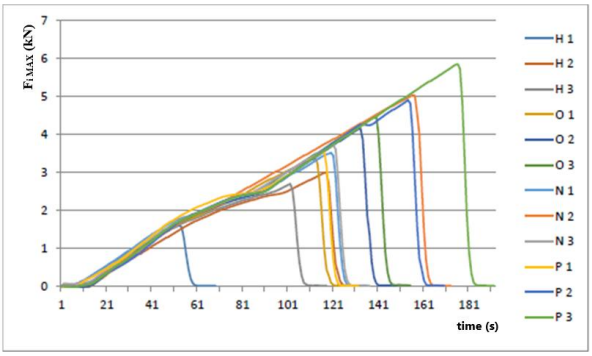


***Fig.7**: Deformation curves*

From the bar graph in Figure 8, it can be seen that the maximum force required to deform the bonded joint is highest for those specimens that had a machined surface. For the structural steel and galvanized sheet specimens, the bonded joint withstood the most when the bonded area was grooved. The stainless steel and aluminum specimens showed the best bonded joint properties when the surface was ground.

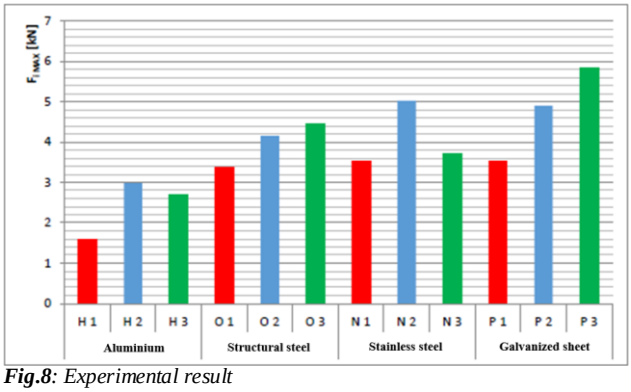


***Fig.8**: Experimental result*

Another criterion for the quality of the bonded joint is the type of fracture remaining after the test (Table 4). The two most common types of fracture were observed in the failed specimens, with one occurring in all types of specimens.

***Table 4**: Resulting adhesive shear strength and fracture type of the bonded joint*

Samples	***τ_i [MPa]***	***Type of material failure***
H1	5,120002271	AF (adhesive failure)
H2	9,552776379	AF (adhesive failure)
H3	8,613856779	AF (adhesive failure)
O1	10,7356372	AF (adhesive failure)
O2	13,28939687	SCF (cohesive failure at the substrate boundary)
O3	14,22704594	90% AF, 10% SCF
N1	11,23622492	AF (adhesive failure)
N2	16,07185144	60% AF, 40% SCF
N3	11,87657063	80% AF, 20% SCF
P1	11,325161182	AF (adhesive failure)
P2	15,66909432	40% AF, 60% SCF
P3	18,69676063	90% AF, 10% SCF

4. Results and conclusions

The use of bonded joints in the automotive industry is widespread nowadays. This tendency is growing, so it is necessary to consider where in the structure this type of connection can be used.

For the shear strength test, which was carried out on a TIRA test 2300 test machine, we had 12 samples (4 groups of samples, each group of samples containing 3 adherends). These samples were tested independently with the same type of bonded joint. The machine testing was followed by processing of the individual measured values. As a result, the best combinations of bonded joint between composite materials and metallic materials were tested and found. The analysis showed that the best combination of bonded joint in shear is composite material and galvanized sheet metal. This combination shows the highest values in the maximum shear stress and maximum strain force indices. On the other hand, the lowest values of maximum shear stress and maximum force are for the combination of bonded joint in shear of composite specimen with aluminum specimen.

For better objectivity and to draw relevant conclusions, it is necessary to test more variants of bonded adherends as well as other types of adhesives at bonded joints. These joints should be tested subsequently for brittleness and impact strength and compared with the measured values from the shear strength test in order to obtain a more meaningful value.

Acknowledgements: The contribution was supported by the Slovak Research and Development Agency; Scientific Grant Agency VEGA 2/0080/19 - Prediction of weldability and compressibility of combined laser welded blanks from high-strength steels with the support of CAE systems

5. References:

1. B.D. Agarwal, J.B. Lawrence. Fiber composites. Prague: SNTL- Nakladatelství technické literatury, 294 p. (1987)
2. R. Bareš. Composite materials. Praha: SNTL, 325 p. (1988)
3. M.D. Banea, M. Rosioara, R.J.C. Carbas, L.F.M. da Silva. Multi-material adhesive joints for automotive industry. Composites Part B: Engineering. Volume 151, 15 October. Pages 71-77 (2018)
4. J. Jančář. Introduction to materials engineering of polymer composites. Brno: Brno University of Technology, Faculty of Chemistry, 193 p. ISBN 8021424435 (2003)
5. P. Skočovský et al. Material science for mechanical engineering. Žilina: University of Žilina in Žilina, 349p. ISBN 8080705933 (2006)
6. STN EN 1465: 2006, Adhesives. Determination of the shear strength of a lap joint under tensile stress. (2006)
7. M. Gregor. Technologie a technika lepení. Lepidla.cz, Available at: https://www.lepidla.cz/cs/a/technologie-a-technika-lepeni--zakladni-informace.html (2021)
8. A. Rivai, K. Diharjo, M. Anwar, R. Tarigan. Effect of Adhesive Thickness and Surface Treatment to Shear Strength on Single Lap Joint AL/CFRP Using Adhesive of Epoxy/Al-fine-powder, Conference: 6th Nanoscience and Nanotechnology Symposium (NNS2015) 1710. 10.1063/1.4941496. (2015)
9. M. Balážiková, M. Tomašková. Objectification and determination of hand-armd vibrations, In: Trans&Motauto World. - Sofia (Bulharsko): Scientific Technical Union of Mechanical Engineering 4/3, p. 87-90. ISSN 2367-8399 (2019)
10. A. Rick. Understanding Adhesive Failures. Available at: https://tombrowninc.com/blog/understanding-adhesive-failures/ (2018)

Estimation of the elasticity module of Al-Si alloy samples in cast and deformed states by the frequency spectrum of sound vibrations

Vladislav Kaverynskyi, Zoya Sukhenko , Gennadii Bagliuk[1]
Frantsevich Institute for Problems in Materials Science, NAS of Ukrane, Kyiv, Ukraine, 03142, Krzhizhanovsky str., 3
gbag@ukr.net

Abstract: *Using fast Fourier transform the frequency spectra of sound vibrations of sound obtained by impacting a suspended material sample were obtained and analyzed. For this, the corresponding short sound files were recorded, which were then subjected to computer analysis. It was found that the frequency spectra of sound vibrations for cast silumin and for those after deformation-heat treatment have a different character. So in these spectra obtained for samples that have passed the deformation-heat treatment, a set of narrow, clearly peaks at certain frequencies have been observed. In the spectra obtained for cast samples, such clear, narrow peaks are not observed. The position of the characteristic peaks in the frequency spectra of sound vibrations was used to estimate the elastic modulus for samples that have passed various regimes of deformation-heat treatment.*
KEYWORDS*: SILUMIN, FAST FOURIER TRANSFORM, ELASTIC MODULUS, DEFORMATION-HEAT TREATMENT*

1. Introduction

The *objective* of this research is to study the effect of deformation-heat treatment of alloys of the Al-Si system on the nature of the frequency spectra of sound vibrations obtained by fast Fourier transforms [1] of a recording sound emitted when hitting a suspended sample, as well as evaluating the elastic modulus of the material studding the values of natural frequencies.

Alloys of the Al-Si system are used for the cast products manufacture and practically do not undergo plastic deformation. This is because of the low ductility of such materials. We have proposed and investigated a method for increasing the plasticity of such alloys by deformation-heat treatment, which consists of a series of small hot deformations with intermediate annealing. As a result of this treatment, the plasticity of the alloy actually increased, and the silicon inclusions were crushed and acquired a shape close to spherical or equiaxial "tumbling" fragments. Annealing without deformation, both simple and cyclic, even for the time of 4–5 h at temperatures above 500 ºC, did not have such a significant effect on silicon inclusions as the combination of a series of hot deformations with intermediate cooling and annealing.

When working with the samples, an interesting detail was noticed – the sound emitted when the sample was struck or dropped onto a hard surface was different for cast and annealed samples, and for samples that underwent deformation-heat treatment. In other words, the samples after forging produced a pronounced prolonged ringing sound; for cast and annealed samples, a short, indefinite rattling was observed. This difference in sound prompted the idea of a more detailed study of this difference. The sound obtained by impacting the samples was recorded and subjected to both the analysis of the time dependence of the vibration amplitude and the Fourier transform to obtain the spectrum of the vibration frequency intensity in the corresponding recorded sound.

2.1. Experimental material and technique

The study used samples of alloys of two types – with 4.5% Si and with 7% Si. The chemical composition of both types of samples is shown in Table 1.

Table 1

Chemical composition of the test samples (wt%)

Sample type	Al	Si	Mn	Cu	Fe
1	base	7.0	0.1	0.5	0.75
2		4.5	0.5	0.7	0.5

The samples had shapes of rectangular rods of various lengths and sections. Table 2 shows the geometric dimensions of the samples. At the same time, it also indicates the type of sample, which depends on the nature of the processing to which it was or was not subjected.

Table 2: *Geometric dimensions of samples, mm*

Sample type by the chemical composition (see table 1)	Sample type by the material state (see table 3)	№ of sample	Sample dimensions		
			a	*b*	*l*
1	1	1	7.8	6.9	59.9
		2	7.9	7.1	52.2
	2	3	6.4	7.2	79.8
		4	6.65	7.5	70.15
2	3	5	7.3	6.5	82.1
		6	7.2	6.1	91.0
1	4	7	5.9	6.6	67.9
	5	8	8.8	8.4	40.8
	6	9	9.4	8.7	41.5
2	5	10	14.2	13.9	37.9
	5	11	13.0	11.5	30.8

Table 3 shows brief characteristics of the sample processing modes, the numbering corresponds to the numbers from the column "Sample type by the material state" in Table 2.

Table 3: *Processing modes for the samples*

№ of treatment type	Processing characteristic
1	11 stages of deformation by forging with intermediate annealing for 12 – 18 minutes at a temperature of 520 ºC. Start of forging at 520 – 510ºC, end of forging at ~ 250 – 300 ºC. The total degree of deformation is ~ 29%, elongation is ~42%.
2	17 stages of deformation by forging with intermediate annealing for 10 – 12 minutes at a temperature of 510 ºC. Start of forging at 510 – 490ºC, end of forging at ~ 100 – 150 ºC. The total degree of deformation is ~ 52%, elongation is ~98%.
3	11 stages of deformation by forging with intermediate annealing for 15 – 20 min at a temperature of 540 ºC. Final annealing 30 min. Start of forging at 540 – 520 ºC, end of forging at ~100 – 200 ºC. The total degree of deformation is ~70%, elongation is ~ 138%.
4	19 stages of deformation by forging with intermediate annealing for 9 – 15 minutes at a temperature of 510 ºC. Start of forging at 510 – 490ºC, end of forging at room temperature. Final cold deformation. The total degree of hot deformation is ~ 33%, the final cold deformation is ~ 12%, and the total elongation is ~ 63%.
5	Initial cast condition

6	Annealing at a temperature of 520 – 540 ºC for ~4.5 h.

The samples were hung on a string, and the sample was struck with a wooden stick. The sound produced by this was recorded and saved as an audio file of the .wav format. This file was passed to a program that performs fast Fourier transforms and visualizes the results as a plot. The program is written in Python, for the implementation of fast Fourier transforms, the functions of the program library numpy [2, 3] were used in it, and matplotlib [4] was used to visualize the results. The resulting graphs were saved as graphic files in .jpg format. The positions of the peaks on the graphs were measured using the jMicroVision program [5]. For each sample, 10-15 such acoustic spectra were recorded to identify and exclude the effects of random noise and to confirm the repeatability of peak locations.

In addition, the study of the microstructure of the samples, measurement of their Vickers hardness, microhardness of the metal matrix and plasticity during deposition were carried out.

2.2. Research results

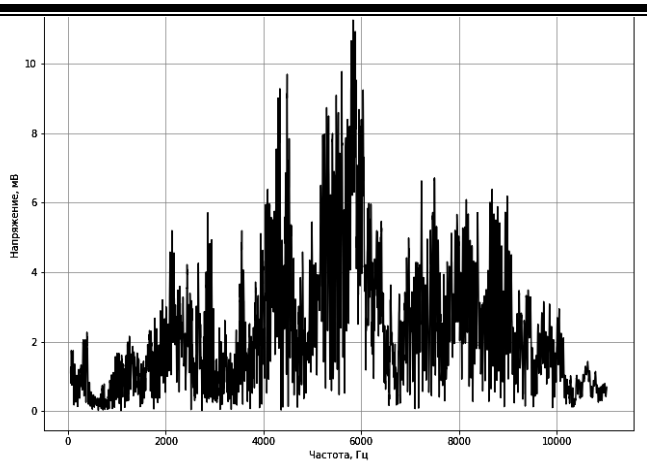
It was noticed that in the acoustic frequency spectra obtained for samples that were subjected to deformation-heat treatment, pronounced peaks appear at certain frequencies. Peaks were observed from time to time at fixed locations for a given sample. The peaks could have different intensities, which in each case, in some cases, individual peaks might not appear at all, but if they appeared it was at the same frequencies. No certain narrow peaks were observed for the acoustic spectra of cast and annealed samples.

Figure 1 shows examples of graphs of acoustic spectra for a cast sample (a) and a sample after deformation-heat treatment (b). In the case of a cast sample, if some peaks can be noticed in the acoustic spectrum, then they are unstable, have low intensity, and their boundaries are blurred.

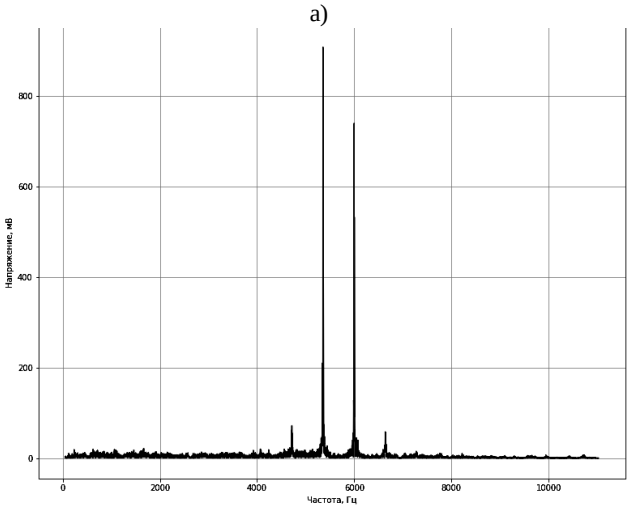
Thus, the first thing that this method allows is to distinguish a specimen in a cast or annealed state from a specimen that has been subjected to deformation-heat treatment.

The observed difference in the acoustic spectra of cast and deformed samples is apparently caused by the difference in the shape of silicon inclusions in them. Figure 2 shows examples of silicon inclusions photographs in cast (a), annealed (b), and deformed (c, d) samples.

Apparently, inclusions of silicon in cast samples, representing a skeleton of silicon wafers, dampen the propagation of sound in the material. In the samples after annealing, the inclusions are more separated, but on the whole retain their plate-like shape. In specimens after deformation-heat treatment, silicon inclusions are globular and to a much lesser dampen the propagation of sound in the metal. In addition, it was noted that in samples with a higher degree of spheroidization of inclusions, the sound, on average, with the same force and nature of impact on the sample, is louder and more sustainable. The hardness of the metal material apparently does not affect the qualitative difference in the frequency acoustic spectra of cast and deformed samples. Thus, the highest hardness was observed in the as-cast state in specimens of composition 1 (67.0 ± 12.1 HB), the hardness of annealed specimens and specimens processed in modes 1 and 2 was lower than in the as-cast state and was about 50 HB. For specimens of composition 2, the hardness in the cast state and after deformation-heat treatment practically did not differ. Thus, we do not observe any significant influence of hardness on the peaks appearance in acoustic spectra and on the degree of their blurring.



a)



b)

Figure1 *– Examples of acoustic frequency spectra – a) cast sample; b) deformed specimen*

It is known from theory that the frequency of sound vibrations of a rod depends on its geometric dimensions and shape, the pattern of its ends pinching, as well as the density and modulus of elasticity of the material [6]. The frequencies of natural vibrations of the rod are described by the formula (1):

$$f = \frac{k}{L^2} \cdot \sqrt{\frac{E \cdot I}{\rho \cdot A}} \tag{1}$$

where L is the length of the rod, m; E is the modulus of elasticity, Pa; ρ is the density of the material, kg/m^3, I is the axial moment of inertia for the cross section of the bar, m^4; A is the cross-sectional area of the bar, m^2, k is a coefficient that depends on the boundary conditions (pinching schemes) and the order of the harmonic.

In this case, the cross section of the sample is rectangular. Thus, there are two axial moments of inertia determined by the formula (2) [7]:

$$I_x = \frac{b \cdot a^3}{12} \qquad I_y = \frac{b^3 \cdot a}{12} \tag{2}$$

where a, b – cross-sectional dimensions, m

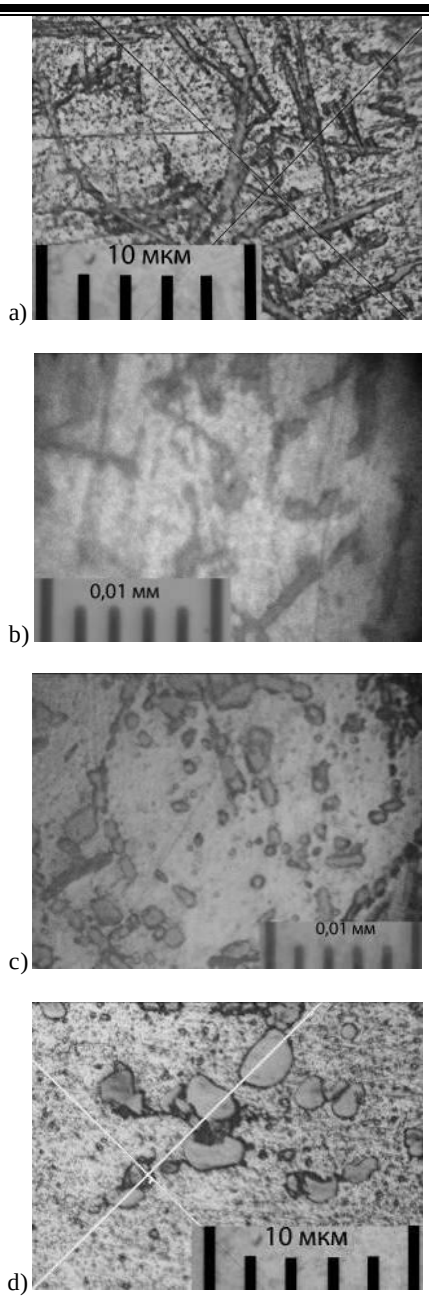


Figure 2 *– Silicon inclusions in silumin samples with 7 % Si:*
a) cast sample, magnification × 500;
b) annealed sample, magnification × 400;
c) sample after deformation-heat treatment, magnification × 400;
d) sample after deformation-heat treatment, magnification × 500;

The presence of two axial moments of inertia leads to split pairs of peaks observed in the frequency spectra of sound vibrations. Also, in a number of cases, harmonics are clearly visible.

By comparing the experimental data with the theory, it was established that for the considered case – a sample hung on a thread – the boundary conditions for the hinge fixation of the ends are most suitable for determining the frequency of natural vibrations. With such a scheme, the coefficient k from formula (1) is $(n \cdot \pi) / 2$, where n is the harmonic number. Most often, the 1st harmonic of natural vibrations (fundamental tone) manifested itself most clearly in the samples, the 2nd one manifested itself relatively seldom (in samples 3, 4, and 7 it was practically not observed), but the 3rd was often intense. The reason for this behavior is still unclear.

Knowing the geometric parameters of the sample and its density, based on the position of the peaks in the acoustic frequency spectrum, it is possible to estimate the value of the elastic modulus of the material, according to formula (1). The material density of the samples of composition 1 was determined to be 2670 kg/m^2, and of type 2 – 2680 kg/m^2. The calculated estimate of the elastic modulus of type 1 specimens processed by mode 1 was 72.0...72.9 GPa, by mode 2 – 75.2...76.2 GPa, and by mode 4 – 78.3...81.1 GPa. This is not a huge but statistically significant difference.

Considering the fact that the hardness of the metal matrix of specimens processed according to mode 2 (48.2±9.8 kgf/mm^2) is slightly higher than that of specimens processed according to mode 1 (41.8±3.8 kgf/mm^2), it is possible to assume the relationship between the modulus of elasticity and the hardness of the metal matrix of the material, while the total hardness practically does not differ. Mode 4 includes additional cold deformation, which increases the hardness of the material. Obviously, its modulus of elasticity increases, as is known, correlates with the hardness of the material [8].

The acoustic frequency spectra for samples of composition 2 (4.5 % Si) are characterized in a similar way: there do not have certain narrow peaks for the cast state, but they appear after deformation-heat treatment. The calculated estimate of the elastic modulus for sample 5, deformed by ~ 70%, is 75.4...75.7 GPa. Although the hardness of these specimens (35.2 ± 5.0 HB) is lower than that of specimens with 7% Si, their estimated modulus of elasticity is approximately at the level of specimens processed according to mode 2. This still indicates a not quite direct dependence of the modulus of elasticity on hardness and, apparently, shows the role of the large degree of deformation to which these samples underwent.

Thus, the considered approach makes it possible to estimate the values of the elastic modulus of the material in a fairly simple way without special equipment.

3. Conclusions

The study has been carried out of the frequency spectra of sound vibrations obtained by fast Fourier transforms of audio files with a recording of the sound emitted when struck by suspended samples of alloys of the Al-Si system. This method was used to study samples with 4.5 and 7.0% Si in cast and deformed states.

A significant qualitative difference in the frequency spectra of sound vibrations for cast and deformed samples is shown. The observed difference is apparently associated with the damping and scattering of sound vibrations by silicon inclusions in the cast material, where they form a frame of lamellar precipitates. The globular shape of silicon inclusions in the material after deformation-heat treatment does not lead to such scattering of sound vibrations; therefore, certain narrow frequencies appear in the acoustic spectrum, corresponding to the natural vibrations of the rod.

The position of the characteristic peaks in the frequency spectra of sound vibrations for the samples after deformation-heat treatment is in good agreement with the theoretically calculated frequencies of natural vibrations of a rod with hinged ends. This makes it possible, knowing the geometric dimensions and shape of the sample and its density, to estimate the value of the elastic modulus of the material.

The evaluation of the elastic modulus carried out on the basis of determining the position of the natural vibration frequencies of the rod (sample) showed that it somewhat increases with an increase in the total degree of deformation during the deformation-heat treatment of the silumin and additionally increases with the combination of the basic multistage hot and final cold deformation. It is also shown that the values of the elastic modulus for samples with 4.5 % of Si after deformation-heat treatment with a total deformation greater degree than that of the samples with 7 % of Si were subjected to, is approximately at the same level as in one with 7 % of Si. Despite the fact that the hardness of this material is noticeably lower.

4. References

1. G. Nussbaumer. Fast Fourier Transform and Convolution Computing Algorithms / G. Nussbaumer – Moscow: Radio and communication, 1985, 248 p. (Rus.)

2. NumPy: The fundamental package for scientific computing with Python. [Electronic resource] Access mode: https://numpy.org

3. Math in Python: Fourier Transform. [Electronic resource] Access mode: http://old.pynsk.ru/posts/2015/Nov/09/matematika-v-python-preobrazovanie-fure/#.X6FOS3Qa-Uk (Rus.)

4. Matplotlib: Visualization with Python. [Electronic resource] Access mode: https://matplotlib.org

5. jMicroVision: User-friendly software for analyzing large images. [Electronic resource] Access mode: https://jmicrovision.github.io

6. N. I. Lavrovich. Natural frequencies of rods oscillation. / N. I. Lavrovich // Omsk Scientific Bulletin. – 2000. – Vol. 12 – P. 106–108. (Rus.)

7. Table. Axial moments of inertia, moments of resistance and radii of inertia of plane figures. [Electronic resource] Access mode: https://tehtab.ru/Guide/GuideMatherials/MaterialsResistant/MomentsOfInertion/ (Rus.)

8. O. M. Dubovyi, Formation of nanosized polygonization substructure and its influence on the physical and mechanical properties of metals, feet and powdered coatings / O.M. Dubovyi, A.A. Karpechenko, M.M. Bobrov, O.O. Zhdanov, T.O. Makrukha, Y.E. Nedelko // Metal Physics and the latest technologies, 2017. – vol. 39, № 2. – P. 209-243. (Ukr.)

The nanostate factor in the technology of polymer nanocomposites

Avdeychik Sergey [1], Goldade Victor [2], Antonov Alexander [3], Struk Vasily [3], Klochko Pavel [3]
Molder Ltd[1] – Grodno, Belarus, Francisk Skorina Gomel State University[2] – Gomel, Belarus,
Yanka Kupala Grodno State University[2] – Grodno, Belarus,
E-mail: antonov.science@gmail.com

Abstract: *Methodological approaches to the implementation of the nanostate phenomenon in the formation of the optimal structure of composite materials and metal-polymer systems at different levels of organization have been developed. The concept of energy and technological compliance of functional composite materials and systems components, which determines the optimal parameters of stress-strain, adhesion and tribological properties under technological influences on the components in the process of obtaining composite and its processing, is proposed.*
KEYWORDS: *NANOPARTICLE, NANOSTATE, METHODOLOGICAL PRINCIPLES, STRUCTURE, ENERGY AND TECHNOLOGICAL COMPLIANCE*

1. Introduction

Modern scientific views on the structure of multicomponent materials (plastics, composites, alloys), products and constructions made on its basis have its foundations in the understanding them as systems whose parameters of characteristics (stress-strain, tribological, thermophysical, adhesive, etc.) depend on the intensity interphase interactions, characterized by the flow of certain physical and chemical processes at a given rate and leading to the formation of boundary (separating) layers with certain composition and structure [1–3]. These processes lead to the transformation of the initial state of the system components and determine the parameters of its performance characteristics.

2. Discussion

In the interfacial region of a multicomponent system, a complex of physical and physicochemical reactions occurs simultaneously with the dominant of one or several, for which the most favorable conditions are realized, determined by the value of the activation energy parameter (Fig. 1). This dominant reaction in the interfacial region, the kinetics of which corresponds to the conditions of formation and operation of the system, determines the resistance of an element made of a composite or a structure to the influence of technological or operational factors.

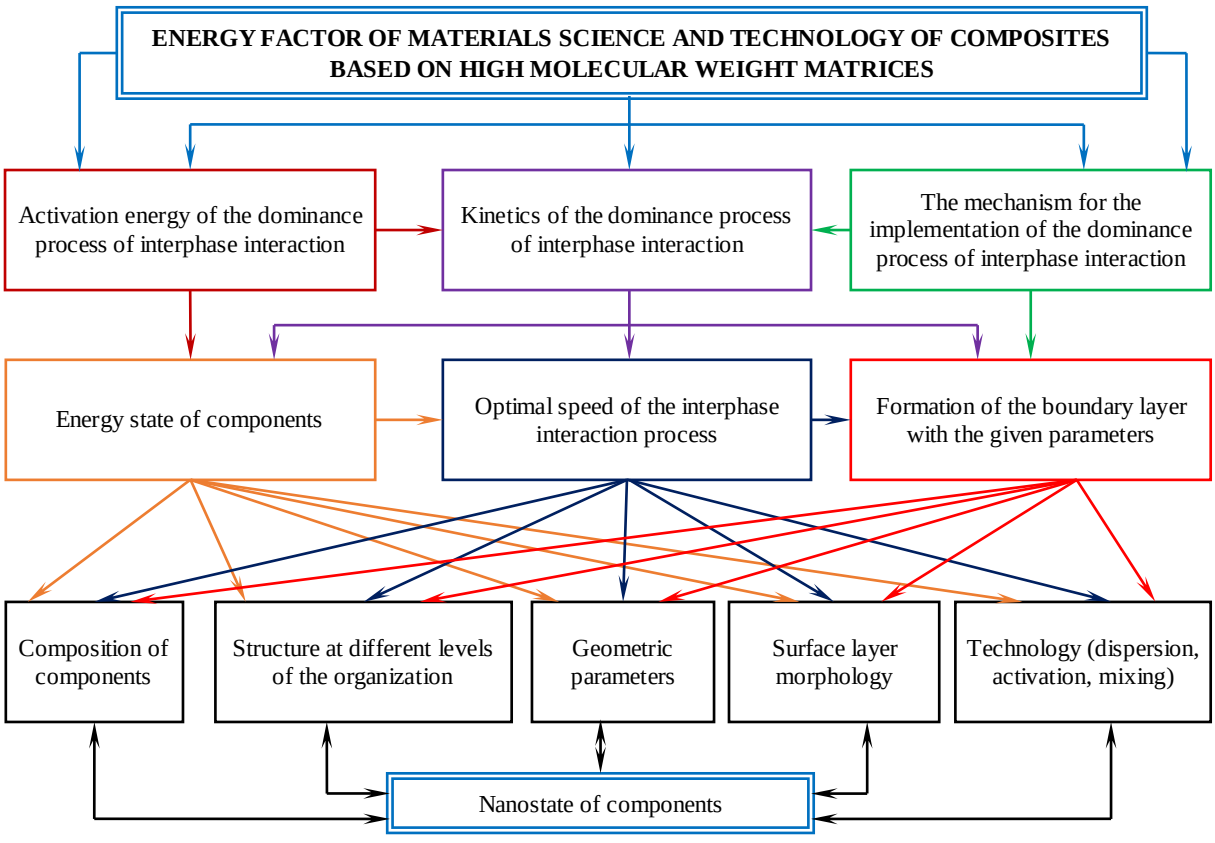


Fig 1. *Energy factor of materials science and technology of composites based on high molecular weight matrices*

Methodological approaches to the creation of composite materials based on polymer matrices in the presence of general regularities are characterized by a number of specific features determined by the modes of operation of the product, requirements for manufacturability and recycling, economic parameters that affect its competitiveness when compared with analogues.

In [4], the directions of targeted modification of polymer materials to improve the tribological characteristics are presented (Fig. 2).

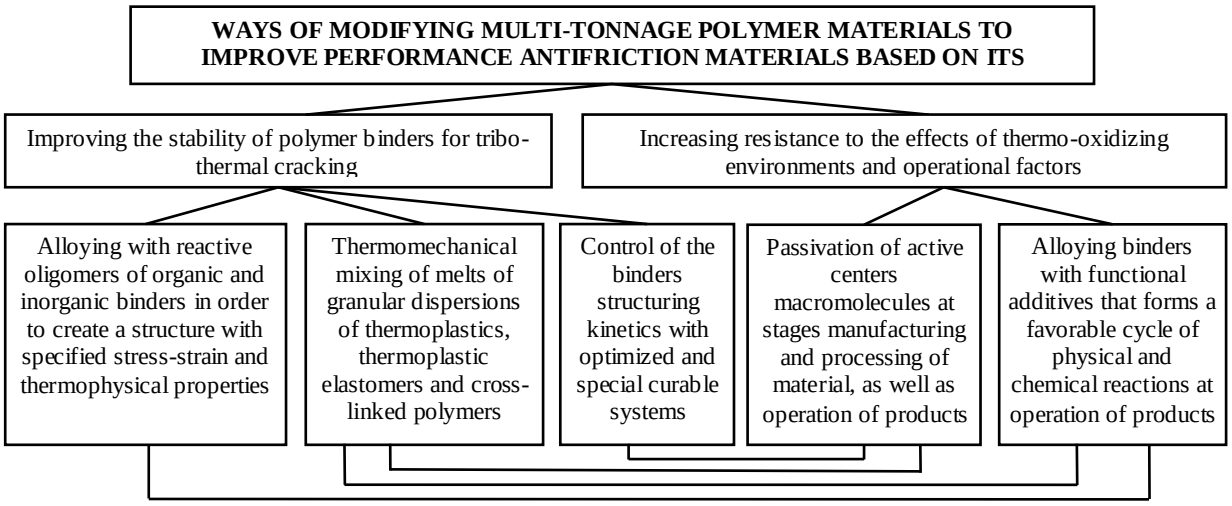


Fig 2. *Some directions of multi-tonnage modification produced polymer materials [4]*

It seems to us that the proposed modification methods are effective not only when creating tribological ("antifriction" according to [4]) materials, but also other types of composites for manufacturing products with specified performance parameters with appropriate adjustments to methodological approaches.

Analysis of numerous methods of targeted modification of high-molecular-weight matrices to obtain functional materials with specified parameters of characteristics, ensuring the effective use of products from them in the structures of machines, mechanisms of technological equipment, not only emphasizes their diversity, but also allows formulating methodological principles for the implementation of functional materials science in accordance with strategy of innovative development of various branches of the economic complex. When developing such principles (Fig. 3), we took into account the current trends in the development of the industrial sphere and the sphere of life support of social-minds of various levels, based on the permanent renewal of industrial products, increasing the level of its consumer characteristics, including ergonomic ones, in the concept of an ecological imperative in the process production and consumption of industrial products, the concepts of reasonable sufficiency and life cycle.

The application of these trends in the practical functional materials science of composites for mechanical engineering made it possible to identify the main requirements, the implementation of which ensures the achievement of optimal technical and social effects:

– optimization of parameters of deformation and strength characteristics;

– increasing the parameters of tribological characteristics in the given operating conditions;

– increasing the parameters of protective characteristics in certain operating conditions.

The formed requirements mainly relate to the field of functional materials science for mechanical engineering and do not consider the features of special materials science, the objects of which are used in the field of housing and communal services, medicine, agricultural production, sports and other areas of the functioning of industrial and special structures.

In our opinion, the formed requirements for functional composite engineering materials based on thermoplastics can be ensured by implementing the basic methodological principles, which include:

– formation of a structure with optimal ordering at a certain level of the organization;

– increasing resistance to tribo-thermal cracking;

– increasing resistance to the effects of thermo-oxidizing and operating environments and aging.

The proposed principles are based on modern approaches to controlling the structural characteristics of composite materials at the molecular, supramolecular, intermolecular and interfacial levels using various materials science and technological solutions, which are systematized by directions:

– doping matrices with reactive components that form chemical bonds between macromolecules;

– introduction into the composition of dispersed, including nanoscale, components of a given composition, habit and energy state into the bulk or surface layers;

– thermomechanical mixing of melts of the matrix and alloying components during the preparation and processing of the composite material;

– mechanochemical mixing of matrix and alloying components during the preparation and processing of composites into a product;

– passivation of active centers of macromolecules in the process of creating and processing composites and the operation of products from its;

– introducing functional additives into the composites, contributing to the formation of favorable cycles of physicochemical, including tribochemical, reactions.

It is obvious that the choice of the direction for the implementation of the methodological principle of creating a functional material with certain parameters of consumer characteristics depends on the purpose and operating conditions of the product from it in the designs of a specific system.

A characteristic feature of the introduced above methodological principles of creating composite materials for products of a certain functional purpose is their direct or indirect relationship, which manifests itself in the simultaneous influence of the selected factor on the complex of structural and physicochemical processes that determine operation under given conditions. For example, the introduction of nanosized modifiers into the composition of the composite simultaneously affects the structural parameters due to the formation of supramolecular formations of a new type, leads to the passivation of the active centers of macromolecules due to the formation of adsorption bonds, and changes the physicochemical processes that determine the adhesion, tribological characteristics, resistance to the effects of thermo-oxidizing environments and aging. Therefore, it is of particular interest to searching for modifiers of the complex mechanism of action, the use of which will allow the implementation of synergistic effects, manifested in the simultaneous increase in the complex of parameters of service characteristics.

The direction of using nanosized particles as a component that passivates the active centers of macromolecules, which creates preconditions for the initiation and development of unfavorable processes of destruction, oxidation, crosslinking, etc., which lead to a qualitative change in the initial structure of the composite with optimal parameters operational characteristics. The development of this approach, previously considered in [4], will make it possible to develop machine-building materials with increased performance parameters based on thermoplastic matrices for large-scale production of the class of polyamides and polyolefins, including

regenerated ones, the use of which currently does not correspond to its requirements potential opportunities.

The developed methodological principles are implemented in practical applications in the form of functional nanomaterials based on industrial thermoplastics and technologies for their manufacture and processing into products [5–8].

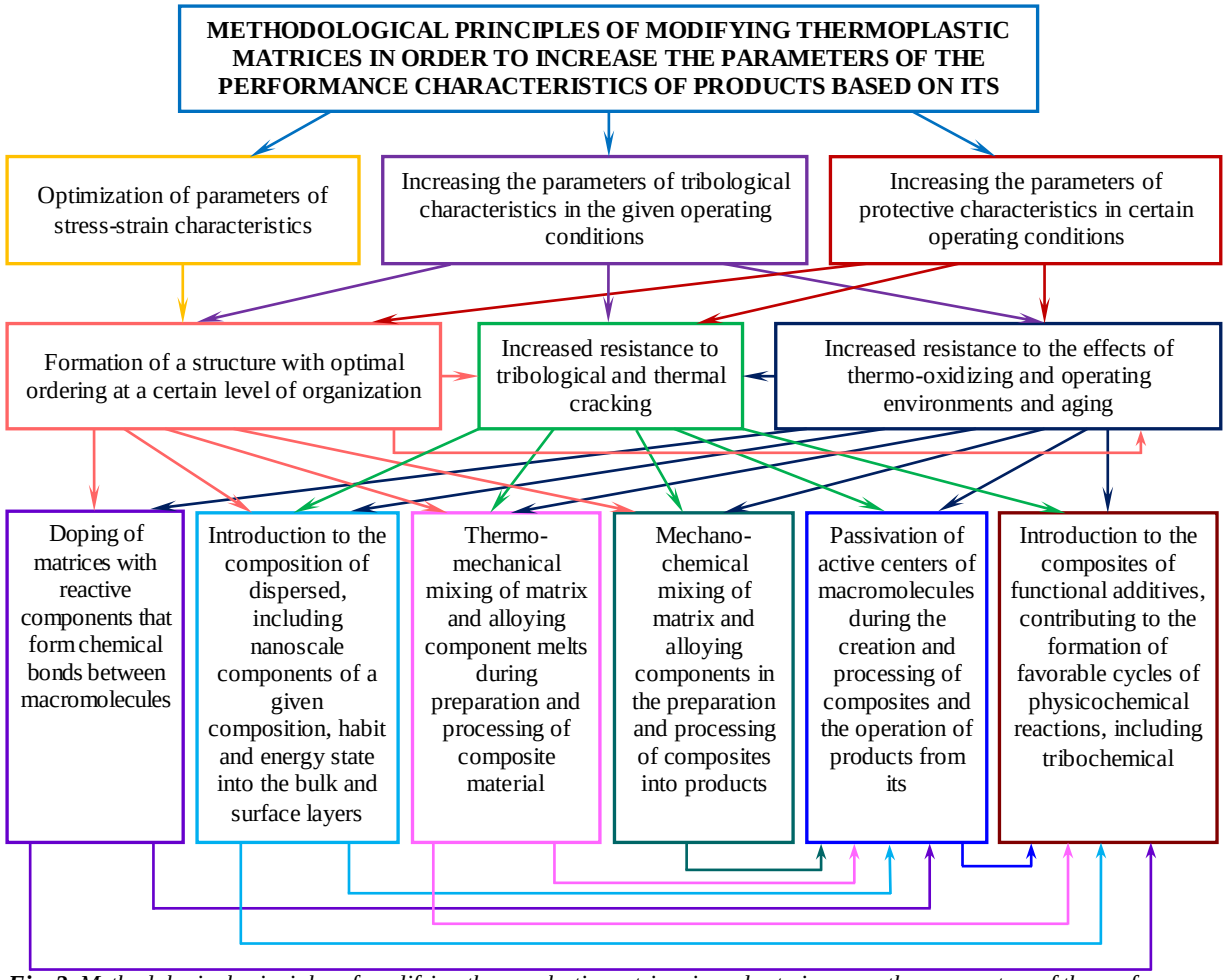


Fig. 3. *Methodological principles of modifying thermoplastic matrices in order to increase the parameters of the performance characteristics of products made from its*

3. Conclusion

Methodological approaches to the implementation of the nanostate phenomenon in the formation of the optimal structure of composite materials and metal-polymer systems at different levels of organization have been developed. The concept of energy and technological compliance of functional composite materials and systems components, which consists in ensuring the parameters of their energy characteristics are adequate to the value of the activation energy of the prevailing structural process is proposed. This concept determines the optimal parameters of stress-strain, adhesion and tribological properties under technological influences on the components in the process of obtaining composite and its processing. The concept was tested in the development of nanocomposites based on polymer matrices of industrial production, which surpass analogues in service characteristics.

4. Acknowledgements

The given research was carried out within the framework of integrated assignment 8.4.1.4 "Mechanisms of directed structure formation of functional thermoplastic composites under energy and mechanical influences" of R&D "Investigation of the multilevel structuring mechanisms of functional nanocomposites based on thermoplastics under conditions of the realization of physicochemical synergistic effects" and R&D "Investigate the structure formation mechanisms of regenerated thermoplastics and develop methods for increasing the parameters of stress-strain and rheological characteristics of functional composites based on its" included in the subprogram “Multifunctional and composite materials” of the State programs for scientific research “Materials science, new materials and technologies” in 2021-2025. Also the given research was carried out within the framework of integrated assignment 5.6 "Research of the processes of creation and use of polymer packaging materials to ensure the quality and safety of food products" of R&D "Investigation of the processes of structure formation of thermoplastic nanocomposites for obtaining film semifinished products with increased parameters of characteristics" included in the subprogram “Food security” of the State programs for scientific research “Agricultural technologies and Food security” in 2021-2025.

5. References

1. Kuleznev V.N. Smesi i splavy polimerov [Mixtures and alloys of polymers]. St. Petersburg, Scientific foundations and technologies, 2013. – 216 p. (in Russian).
2. Mikhailin Yu.A. Konstruktsionnye polimernye kompozitsionnye materialy [Structural polymeric composite materials]. Scientific foundations and technologies, 2008. – 822 p. (in Russian).
3. Eliseev A.A., Lukashin A.V. Funktsional'nye nanomaterialy [Functional nanomaterials]. Moscow, Fizmatlit, 2010. – 456 p. (in Russian).
4. Struk V.A. Tribochemical concept for the creation of antifriction materials based on multitonnage polymer binders [Tribokhimicheskaia kontseptsiia sozdaniia antifriktsionnykh materialov na osnove mnogotonnazhno vypuskaemykh

polimernykh sviazuiushchikh: dis. … d-ra tekhn. nauk]. Minsk, 1988. – 325 p. (in Russian).
5. Avdeychik S.V., Liopo V.A., Ryskulov A.A., Struk V.A. Vvedenie v fiziku nanokompozitsionnykh mashinostroitel'nykh materialov [Introduction to the physics of nanocomposite construction materials]. Grodno, GGAU, 2009. – 439 p. (in Russian).
6. Struk V.A., Prushak V.Ya., Avdeychik S.V., Liopo V.A., Dmitrochenko V.V., Protasenya A.V. Polimer-silikatnye mashinostroitel'nye materialy: fiziko-khimiia, tekhnologiia, primenenie [Polymer-silicate construction materials: physical chemistry, technology, application]. Minsk, Tekhnalogiya, 2007. – 431 p. (in Russian).
7. Avdeychik S.V., Kostyukovich G.A., Krav-chenko V.I., Lovshenko F.G., Lovshenko G.F., Panteleenko F.I., Rogachev A.V., Struk V.A., Tochitskiy E.I. Nanokompozitsionnye mashino-stroitel'nye materialy: opyt razrabotki i primeneniia [Nanocomposite construction materials: development and application experience]. Grodno, GrSU, 2006. – 403 p. (in Russian).
8. Avdeychik S.V., Struk V.A., Antonov A.S. Faktor nanosostoianiia v materialovedenii polimernykh nanokompozitov [The nanostate factor in the material science of polymer nanocomposites]. Saarbrücken, LAP LAMBERT Acad. Publ., 2017. – 468 p. (in Russian).

State and prospects of application of plastically deformed nanostructured metals, alloys, and sprayed coatings

Syzonenko Olha[1, 2], Dubovyi Oleksandr[2], Makrukha Tetiana[2], Karpechenko Anton[2], Bobrov Maksym[2], Torpakov Andrii[1]
Institute of Pulse Processes and Technologies of the National Academy of Sciences of Ukraine – Mykolaiv, Ukraine [1]
Admiral Makarov National University of Shipbuilding – Mykolaiv, Ukraine [2]
sizonenko43@rambler.ru

Abstract *It is shown that thermal stabilization of the polygonization substructure up to 60 min is provided by a combination of uniaxial compressive deformations, namely dynamic by 30% and static by 30%, followed by pre-recrystallization heat treatment (PHT) at the initial recrystallization temperature. This ensures subgrain size of 80… 187 nm, while strength characteristics increase by 10… 30% with sufficient ductility.*
It is shown that PHT provides the formation of nanoscale elements in electric arc coatings with Sv-08G2S (Св-08Г2С), and additional deformation of the coating allows to increase the thermal stability of the polygonization substructure up to 40… 50 min.
It is found that the combined deformation and subsequent PHT of steels provides an increase in the calculated number of nanoscale subgrains from 15 to 65%.
Keywords*: PRE-CRYSTALLIZATION HEAT TREATMENT, SUBGRAIN SIZE, POLYGONIZATION, HARDENSS, DYNAMIC DEFORMATION, STATIC DEFORMATION*

1. Introduction

Modern industry is constantly in need of new technologies and materials that can improve the properties and working life of various products. The use of new materials in structures and individual parts is determined by the relationship between strength and ductility of metals and alloys, as well as wear resistance, which is provided mainly by coatings with a suitable structure. The increase in strength, which also forms increased wear resistance with sufficient plasticity, is provided mainly by the formation of a dispersed micro- and nanoscale structure [1, 2].

Grinding of the grain (subgrain) structure to nanoscale size is performed mainly by the conventional methods of intense plastic deformation (IPD), which forms a highly disoriented fragmented substructure due to the large deformation [3, 4]. Volumetric nanostructuring by IPD methods is used in engineering to obtain small products [2]. The task of creating an effective IPD device that will provide low-complexity production of massive nanostructured blanks and products with high properties will be relevant for a long time.

In recent decades, methods of mechanothermic and thermomechanical treatment were developed and used, which significantly improved the quality of rolled and forged steel products by forming a dispersed polygonization substructure [5]. High-temperature thermomechanical treatment, for example, of high-carbon steels allows to form the dispersed polygonization substructure, which leads to the rise of strength by 30… 60% while maintaining sufficient toughness [5]. In addition, the polygonization substructure complicates the movement of dislocations in the process of creep [5]. But the possibilities of forming a disperse and nanoscale substructure are not fully used due to the processes of dynamic and collective polygonization, which occur at a relatively long times of exposure to high temperatures.

There are methods of deformation-heat treatment of metals and alloys [6], which provide increase of hardness of metals and alloys, deformed by compression, and sprayed coatings with the decrease of thermal conductivity. This is achieved by heating metal products, alloys and sprayed coatings before the initial recrystallization with short-term (up to 10 min) exposure and subsequent cooling to ambient temperature at a rate less than 5 °C / s, which prevents the growth of subgrains (pre-recrystallization heat treatment). This leads to a formation of disperse and nanoscale polygonization substructure. But short-term exposure means that these methods could not be used to process massive and large metal parts which require large treatment times in order to ensure their volumetric heating.

Therefore, the **goal of the work** is to find the regularities of formation of thermally stable polygonization nanoscale subgrains in metals, alloys and sprayed coatings with high physical and mechanical properties.

2. Methodology

Iron is the main component of any steel, so initial studies of the patterns of influence of deformation and thermal factors on the physical and mechanical properties of metals and alloys were studied on the example of technically pure iron. Specimens of 5 × 5 × 8 mm size were subjected to static deformation on LosenHousenWLRK (Dusseldorf) hydraulic press with a load of up to 35 t. Pre-recrystallization heat treatment (PHT) was performed in SNOL-1.6.2.0.08 / 9-M1 (СНОЛ-1.6.2.0.08/9-М1) laboratory electric furnace. Hardness was determined according to DSTU ISO 6507-4: 2008 (ДСТУ ISO 6507-4:2008) on a Vickers device with a load of 5 kg.

3. Results and discussion

As a result of numerous experiments, information was accumulated to construct a graphical dependence of hardness (HV_5) on the degree of deformation and temperature and the dependence of hardness on the degree of deformation and holding time at the temperature of 500 °C. It is known, for example [7], that a decrease in grain size (subgrain size) leads to an increase in hardness. This effect is observed for almost all types of materials. Strength in most cases increases similarly to hardness, so hardness can be an approximate criterion of strength, as well as it can be used to characterize the size of the subgrain. Moreover, our studies of the effect of pre-recrystallization heat treatment on the grain size of metals and alloys did not record an average grain size of less than 50 nm. The influence of deformation-thermal factors on the hardness (HV5) of technically pure iron is shown in Fig. 1 and Fig. 2.

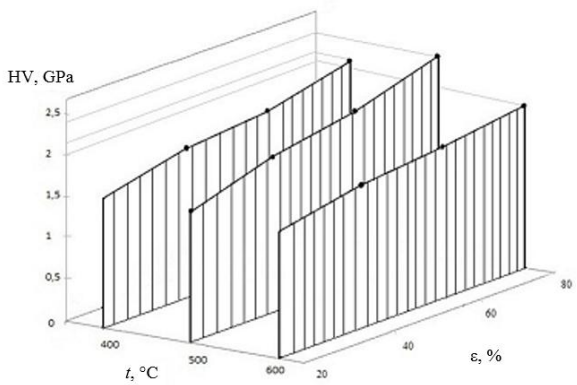


Fig. 1 *The dependence of technically pure iron hardness on the degree of deformation (ε, %) and temperature (t, °C)*

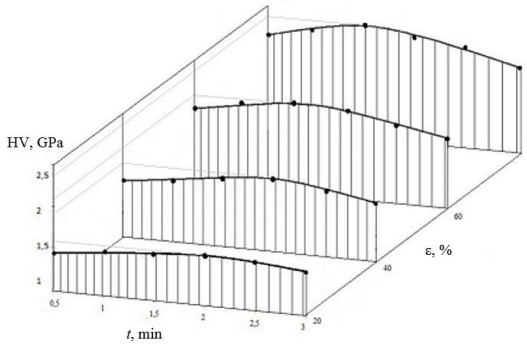


Fig. 2 *The dependence of technically pure iron hardness on the degree of deformation (ε, %) and time of exposure at the temperature of 500 °C (t, min)*

The data of Fig. 1 indicate that the optimal temperature of the pre-recrystallization treatment is 500 °C, while the dependence is extreme, and the maximum hardness is achieved at the exposure for 1.5… 2 min (see Fig. 2). Increasing static deformation leads to the increase of the hardness, which reaches a maximum value at a deformation of 80%. The effect of higher static deformation has not been studied because cracks were observed sometimes during deformation of about 90%, and in practice static deformation above 80% is virtually not used. The maximum observed value of hardness after 80% deformation and PHT at the temperature of 500 °C was 2.4. GPa (after deformation – 1.52 GPa). Thus, the increase in hardness after PHT was 58%. This effect is due to the dispersion of subgrains.

For comparison, specimens of technically pure iron were subjected to triaxial deformation by the "abc" method, as a kind of equal-channel angular pressing [8]. The hardness (HV_5) and the size of the regions of coherent scattering (RCS) of X-rays of specimens of technically pure iron, deformed by the "abc" method and uniaxial compression by 82% after PHT, are shown in table 1. RCS was determined by the Scherrer formula by reflection [110], X-ray diffraction patterns were recorded on a DRON-3.0 (ДРОН-3,0) device. The total value of the actual deformation for the "abc" method was $e = 3.4$.

Table 1: *HV_5 hardness and RCS size of technically pure iron, deformed by "abc" method and by uniaxial pressing after PHT.*

Deformation method	Hardness, GPa, after		*RCS size, nm, after*	
	deformation	deformation and heat treatment	deformation	deformation and heat treatment
"abc"	2.96	3.29	149	72
Uniaxial pressing after PHT	2.35	3.60	83	66

Table 1 shows that after "abc" deformation the hardness is higher if compared to the hardness of specimens after uniaxial deformation, but after pre-recrystallization heat treatment greater hardness is observed in uniaxially deformed specimens. The size of the RCS, which can be used to evaluate the size of the subgrain, has significantly lower values both after uniaxial deformation and after deformation with "abc" method and PHT. It is known, for example [5], that during deformation the movement of dislocations is carried out by sliding and diffusion crawling, thus volume dislocation plexuses are formed, which ensures cellular structure of the material. Under the action of elastic stresses when heated, dislocation plexuses turn into flat small-angle subboundaries, and cells turn into subgrains, but subgrain differs sharply in size, curvature of boundaries, and angles at the triple junctions of subboundaries. The cellular structure formed after the "abc" deformation is transformed into a subgrain. These subgrains are chaotically disoriented relative to each other in contrast to naturally disoriented grains after uniaxial deformation. As a result, the algebraic sum of disorientation of subgrains is almost zero, which leads to the growth of large subgrains from smaller ones and causes a decrease in hardness [5]. In addition, the "abc" deformation is triaxial and thus causes the appearance of more dislocations of various signs, which causes their annihilation. This also leads to the increase of subgrains growth rate. Therefore, the size of the RCS after static deformation and heat treatment is smaller than after the deformation by the "abc" method and heat treatment.

Lower values of hardness of technically pure iron after "abc" deformation and PHT in comparison with uniaxial deformation can also be explained by additional influence of grain boundary sliding. In paper [9] it is indicated that in layers with a subgrain size of 50 to 200 nm the deformation is carried out by a mixed mechanism– the mechanism of grain boundary slippage joins the usual dislocation mechanism. In this case, the deformation can occur by the rotation of the subgrains, which is caused by high level of stresses in the triple joints, which is characteristic to the "abc" deformation.

From a practical point of view, it is advisable to investigate the physical and mechanical properties of technically pure iron and steel. The results of such studies are given in [6, 8], from which it follows that the tensile strength of technically pure iron and steel after PHT in a mode that provides maximum hardness, significantly higher than even after deformation. At the same time it relatively increased the plasticity of specimens. This is due to the fragmentation of the substructure, which is confirmed by the size of the RCS, which lies at the nanoscale range.

PHT makes it possible to increase the hardness (HV_5) of cold-formed Ni80Cr20 nichrome by 25%, of BrAMts9-2 (БрАМц9-2) bronze – by 19%, of M1 electrotechnical copper – by 13%, and of nichrome, sprayed by electric arc – by 29%.

During the spraying of gas-thermal coatings, there is an intense plastic deformation of particles due to the high velocity of the impact with the substrate. In real spraying processes this velocity can reach up to 300 m/s. The amount of deformation can be 90… 95%, and the cooling rate of the deformed particles reaches 108 °C/s, which prevents dynamic recrystallization in the coating material. Short-term exposure of samples with sprayed coatings at the recrystallization temperature and subsequent accelerated cooling in air provides an increase in the hardness of the coatings by fixing the pre-recrystallization state of the coating material.

Electric arc coatings made of Sv-08G2S (Св-08Г2С) wire were studied, because they are characterized by the lowest value of RCS and the highest effect of increasing hardness after pre-recrystallization heat treatment. From a practical point of view, the main disadvantage of pre-recrystallization heat treatment is the short exposure time (a few minutes). Therefore, it is important to study the possibility of stabilizing the dispersed polygonization substructure of the sprayed coating with a longer exposure in the process of heat treatment using subsequent deformation.

In order to inhibit the movement of dislocation subboundaries in the process of collective polygonization, which is manifested by heating (long exposure), additional deformation of the coating was carried out in two ways: by pressing on a hydraulic press at a load of 10 t (30% deformation) and by surface plastic deformation (SPD) with steel balls with a diameter of 0.1-0.3 mm for 2 minutes. The heating temperature of the deformed samples was reduced to 400 °C due to the fact that increasing the values of deformation leads to the decrease of the temperature threshold of recrystallization. The results of these studies are shown in Fig. 3.

Analysis of obtained results shows that the use of the subsequent deformation provides a smaller decrease in hardness while increasing duration of exposure during pre-recrystallization heat treatment to 15 minutes. This trend is observed for both types of deformation of the coating. For example, the hardness of the coating without subsequent deformation when increasing the

duration of exposure from 2 to 15 min decreases from 2.7 to 2 GPa (– 35%), and with the subsequent deformation – from 3 to 2.8 GPa (–7%) and from 3.1 to 3 GPa (–3%) for SPD and pressing, respectively.

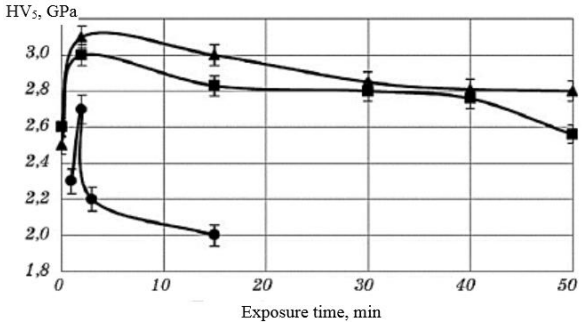


Fig. 3 *The dependence of the hardness of electric arc coatings of Sv-08G2S (Св-08Г2С) wire on the duration of exposure and the type of subsequent deformation without additional deformation at the temperature of 450 °C (●), after SPD(■) and pressing (▲)*

In general, sufficiently high hardness values are ensured at a holding time of up to 40 min for SPD and of up to 50 min for pressing. This is explained by the fact that during re-deformation the dislocation interaction ends with the appearance of 50% to 75% of dislocation barriers, and the rest of dislocations participate in the formation of dislocation plexuses. These dislocation barriers, which arise along the direction perpendicular to the axis of deformation, inhibit the movement of dislocations and, consequently, reduce the mobility of polygonization subboundaries, which reduces the speed of polygonization processes and provides a stabilizing effect. Analysis of microstructures on an optical metallographic microscope showed that no changes in the structure of the coatings before and after heat treatment were detected. This indicates that the strengthening effect is provided by substructure elements.

It is known [5] that grinding the structure and obtaining nanosized elements leads to a decrease in the thermal conductivity of the metal material. Therefore, a study of the effect of pre-recrystallization heat treatment on the thermal conductivity of the obtained electric arc coatings was performed. The analysis of the obtained results showed a decrease in the thermal conductivity of coatings by an average of 15% after pre-recrystallization heat treatment, which is explained by the increase in the length of the subboundaries. In order to perform the quantitative evaluation of the effect of pre-recrystallization heat treatment on the substructure of electric arc coatings, the size of the regions of coherent scattering of X-rays was determined (see Table 2).

Table 2: *The size of the areas of coherent scattering of X-rays of electric arc coatings of Sv-08G2S wire.*

Spraying technology and the amount of deformation of particles	Thermal treatment	RCS size, nm
By conventional technology. Deformation of 83%.	Without thermal treatment	>200
	450 °C, 2 min	106
Using electric pulse impact. Deformation of 87%.	Without thermal treatment	~200
	400 °C, 1 min	87

The data, given in Table 2, indicates a significant effect of PHT on the size of subgrains, especially when using electric pulse action when spraying coatings. After PHT, the size of subgrains (RCS) becomes nanoscale. However, the effect of increasing the physical and mechanical properties of steels was previously implemented only for small products (knives for cutting mica tape and harvester knives, 3… 5 mm thick) because of a short exposure time of 1.5… 2 minutes.

PHT provides an increase in physical and mechanical properties due to the fixation of the dispersed polygonization substructure by short-term exposure of statically deformed metals and alloys at the temperature of primary recrystallization. Prolongation of the exposure time or increase in temperature lead to the leveling of the obtained results through the development of collective polygonization processes. The boundaries of subgrains, formed at the beginning of polygonization, are of dislocation nature. These dislocations are mobile and with increasing temperature or increasing exposure time, without encountering obstacles, they move easily (creep), while increasing the size of subgrains, which leads to the decrease of hardness and strength. All this makes it impossible to apply PHT process to parts of large (more than 10 mm) cross section. Thus, in order to expand the possibility of using PHT for metal products, it is necessary to create obstacles to the movement of dislocations in the form of double and triple intersections, dispersed allocations, etc.

Since St3 (Ст3) steel is one of the most common structural materials used for the manufacture of load-bearing welded structures, so there is scientific and practical interest is the study of changes in the substructure and properties of specimens of St3 (Ст3) steel after combined deformation (CD). Specimens with a size of 3 × 5 × 5 mm were subjected to combined deformation (30% dynamic and 30% static) followed by PHT (t = 500 °C). The speed of dynamic deformation was 100 mm/s, and for static it was 0.5 mm/s. The hardness after deformation of the rock was 1.92 GPa. The dependence of St3 steel hardness on the duration of exposure during PHT is shown in Fig. 4.

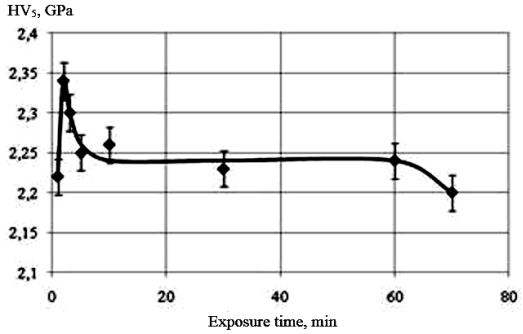


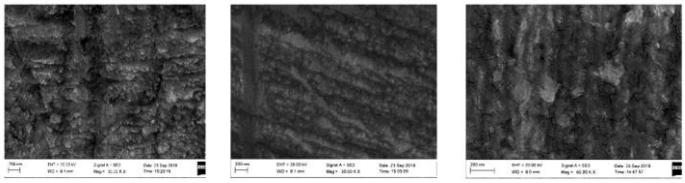
Fig. 4 *The dependence of St3 (Cm3) steel hardness on PHT exposure time*

Fig. 4 shows that the dependence of hardness on the duration of PHT exposure is extreme. The increase in hardness after PHT, which provides maximum hardness, relative to the deformed state is 22%, and after PHT during 60 min it is 17%. Tensile tests were performed (GOST 1497-84) in order to study the changes in temporary resistance to failure, relative narrowing and elongation, the results of these tests as well as evaluation of nanosized subgrain size and quantity are given in table. 3.

Table 3: *The values of temporary fracture toughness, ductility, average subgrain size and the quantity of nanosized elements of St3 (Cm3) steel depending on the type of deformation and heat treatment.*

Treatment type	σ_b, MPa	δ, %	Ψ, %	Average subgrain size, nm	Nanosized subgrains quantity, %
Combined deformation (CD)	310	1.05	74	94	55
CD, followed by PHT, which provides maximum hardness	586	5.26	75	89	66
CD followed by PHT during 60 minutes	402	7.5	59	92	62

Photographs of the substructure of the specimens were obtained using the analytical auto-emission scanning electron microscope SUPRA55VP (see Fig. 5).



a *b* *c*

Fig. 5 *Microstructures of St3 (Cm3) steel) after CD (a), after CD and heat treatment, which provides maximum hardness values (b) and after CD and heat treatment, which provides thermal stabilization of the polygonization substructure (c)*

Figure 5 shows that the substructural elements are dispersed after PHT relative to the deformed state, which is confirmed by the results of the determination of the average size of CSR with a shape factor of ~ 0.42 and by the relative number of nanosized subgrains (see Table 3), which were obtained by computer metallography using ImageProPlus software. The average diameters of subgrains are measured at intervals of 2 degrees and pass through the centroid of the object.

The effect of combined deformation on the average size of subgrains of technically pure iron and individual steels, which are most widely used in industry, was also studied (see Table 4).

Table 4: *The results of determining the size of the CSR of steels after deformation and pre-recrystallization heat treatment*

Treatment type	CSR size, nm					
	Technically pure iron	1020 steel (сталь 20)	1045 steel (сталь 45)	W108 steel (У8)	5140H steel (40Х)	S42000 steel (20Х13)
Combined deformation (CD)	186	143	110	130	131	117
CD, followed by PHT, which provides maximum hardness	125	119	80	115	117	101
CD followed by PHT during 60 minutes	175	187	179	130	118	110

Results, shown in Table 4, indicate that the combined deformation followed by PHT improve the physical and mechanical properties of steels due to the dispersion of substructural elements.

Steels, deformed by the combined method, are characterized by certain features of the structure, which differs significantly from the structure of the same materials that were statically deformed, due to extremely non-equilibrium conditions of their formation (high rate of deformation).

The possible direction of implementation of the proposed technology of combined deformation followed by pre-recrystallization heat treatment and its comparison with traditional technologies of steel products processing is considered on the example of elastic elements.

Springs usually work in the conditions of repeated loadings. In addition to high hardness and strength under static, dynamic and cyclic loads, such parts must have high elastic properties and withstand a large number of repeated loads during operation without breakage and without deposition. This means that when the loads are removed, the spring must fully restore its original dimensions and shape.

The results of the work were implemented at the enterprises of AMIKO DIGITAL LLC, Advice You World GmbH LLC (Ukraine), SAKENA LLC in the production of regulating springs of membrane valves of pipelines. Implementation results have shown that HRC hardness of springs after the proposed deformation and heat treatment is 19% higher than after the application of traditional technology (hardening and tempering).

4. Conclusions

1. It was found that static deformation provides greater efficiency of PHT than equal-channel angular pressing. PHT provides an opportunity to significantly strengthen metals, steels and sprayed coatings with short-term exposure at the temperature of the initial recrystallization (1… 2 min).

2. It is shown that thermal stabilization of the polygonization substructure up to 60 min is provided by a combination of uniaxial compressive deformations, namely dynamic by 30% and static by 30%, followed by pre-recrystallization heat treatment at the initial recrystallization temperature. Such treatment ensures subgrain size in range of 80… 187 nm, while strength characteristics increase by 10… 30% with sufficient ductility.

3. It is shown that PHT provides the formation of nanoscale elements in Sv-08G2S (Св-08Г2С) wire electric arc coatings, and additional deformation of the coating allows to increase the thermal stability of the polygonization substructure up to 40… 50 min.

4. It is shown that the combined deformation and subsequent pre-recrystallization heat treatment of steels provides an increase in the calculated number of nanoscale subgrains from 15 to 65%.

5. Industrial implementation of the proposed method of combined deformation, followed by pre-recrystallization heat treatment for 60 min, on 1070 steel (сталь 70), which is used for the manufacture of control springs of diaphragm valves in industrial conditions, showed that HRC hardness of springs after the proposed deformation and heat treatment is 19% higher than after the application of traditional technology (hardening and tempering). This opens the possibility of practical application of the proposed method of nanostructuring by forming a dispersed polygonization substructure by pre-recrystallization heat treatment.

5. References

1. N.P. Lyakishev, Vestnik Rossijskoi academii nauk. **73**, No. 5. 422 (2003). (In Russian).

2. R.Z. Valiev, I.V. Aleksandrov, *Obyomnye nanostrukturnye metallicheskie materialy: poluchenie, struktura i svoistva* (Akademkniga, Moscow, 2007). (In Russian).

3. V.V. Stolyarov, R.Z. Valiev. Metally, **2**. 5 (2004).

4. K. J. Kurzydlowski, Materials Science. **42**, Issue 1. 85–94 (2006).

5. S.S. Gorelik, S.V. Dobatkin, L.M.Kaputkina, Rekrystallizatsiya metallov i splavov (Moscow: MISiS:2005). (In Russian).

6. O.M. Dubovyi, A.A. Karpechenko, M.M. Bobrov, O.O. Zhdanov, T.O. Makrukha, Yu.Ye. Nedelko, Metallofizika i noveishie tehnologii. 39, No. 2. 209–243 (2017). (In Ukrainian).

7. V.V. Skorohod, I.V. Uvatova, A.V. Ragulya, *Filyko-khimichna kinetyka v nanostrukturnykh systemakh* (Academknyga, Kyiv, 2001). (In Ukrainian).

8. O.M. Dubovyi, S.I. Shkurat, T.O. Makrukha, Zbirnyk naukovukh prats Natsionalnoho universytetu korablebuduvannya. **1**. 36–40 (206). (In Ukrainian).

9. A.I. Yurkova, A.V. Belotskii, A.V. Byakova, Yu.V. Milman, Nanosistemy, nanomaterialy, nanotehnologii. **7**, No. 2. 619–632 (2009). (In Russian).

Investigation of the causes of corrosion of galvanized steel pipes used for hot water supply

Rasa Kandrotaitė Janutienė[1], Darius Mažeika[1]
Faculty of Mechanical Engineering and Design – Kaunas University of Technology[1], Lithuania
E-mail: raskand@ktu.lt, darius.mazeika@ktu.lt

Abstract: *The object of the study is the part of the galvanized steel pipe (about 1-meter-long) supplied by the customers, which was used to supply hot water inside the residential building and which has corroded during exploitation of 5 years. To clarify the situation, quality of surface coating and microstructure of the obtained galvanized steel pipe was analysed. Electrical stray currents of the pipeline installed in the building were measured. The sample of the hot water was taken and analysed at the certificated laboratory.*

The aim of the investigation was to determine the possible causes of the hot water supply pipe corrosion during sufficiently short time of exploitation.

Keywords: GALVANIZED STEEL PIPE, HOT WATER SUPPLY, CORROSION, MICROSTRUCTURE, ELECTRICAL STRAY CURRENTS.

1. Introduction

Despite of increased use of plastic pipes for construction of both cold and hot water supply systems, steel pipes remain at high place on the designing of water supply systems due to technological advantages in laying external water supply systems, as well as high fire safety [1]. The main advantages of steel pipes are their strength, low coefficient of linear expansion, possibility to use several types of pipes connection in one network. However, low corrosion resistance of steel pipes, both ferrous and galvanized, significantly reduces the above advantages.

The protection obtained by zinc-base coatings is due to both barrier and galvanic effects, the last being due to the fact that zinc is anodic to iron and, in humid or aqueous environments it behaves as sacrificial material at discontinuities in the coating. A relevant feature of this type of protection in water supply systems is that, in the presence of carbonates or bicarbonates (normal constituents of hard water supplies), steel corrosion can be decreased by the deposition of insoluble layers on the exposed zones of the inner surface of the steel as a consequence of sacrificial zinc dissolution [2]. However, the soft water inside the supply systems can act contrary, especially, when the temperature of the water is increased [3, 4].

Others criteria that may cause the corrosion of steel pipe lines are AC and DC stray currents. It has been reported that it may occur at induced AC voltage levels of only a few volts [5]. Application of increased cathodic protection current may be required to control AC corrosion.

The object of investigation is the corrosion failure of water supply galvanized steel pipe system at the residential building after short (5 years) lifetime exploitation. The aim of investigation is to determine the possible reasons of the corrosion failure of the galvanized steel pipe.

2. Methodology

The measurement of electrical stray currents of the water supply steel pipe line system was performed using such equipment:

- Portable computer oscilloscope Picoscope 3424,
- Portable oscilloscope FLUKE 123 Industrial Scopemeter,
- For analyzing of the results obtained: HP Pavillion dv6 Notebook PC with Manufacturer's Supplied Software.

The pipeline parts were connected in an electrical chain according to the diagram shown in Fig. 1, a. Voltage measurements were performed at the pipeline installation place according to the following scheme:

- When the Picoscope 3424 portable computer oscilloscope was connected to the hot water pipeline and ground (Fig. 1, b).

Tests of chemical composition and other properties of hot and cold water samples were performed in an accredited laboratory situated in Lithuania. Methods of sample preparation and analysis:

- Testing of chemical composition and other properties of water samples in an accredited laboratory according to standards: LST ISO 6059: 1998, LST ISO 6059: 1998 / P: 2008, LST ISO 6058: 1998, LST ISO 6058: 1998 / P: 2008, LST EN ISO 10304 -1: 2009, LST EN ISO 10523: 2012 (Except p. 8), LST EN 27888: 1999 and LST EN ISO 9963-1: 1999 (Except p. 8.1).

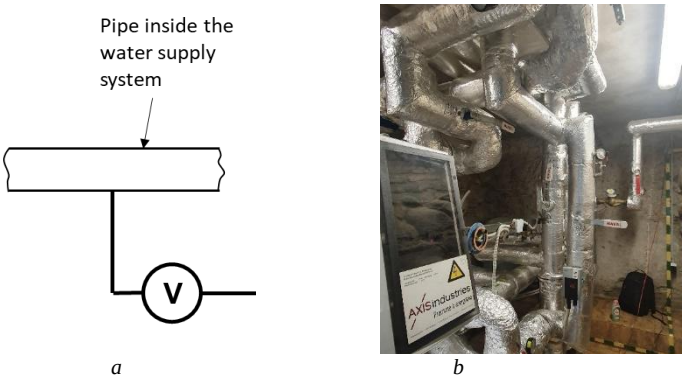


Fig. 1. *Voltage measurement in the hot water pipeline: a - connection diagram of the Picoscope 3424 portable oscilloscope, b - voltage measurement in the hot water pipeline after connecting the circuit according to diagram a*

The data of water sample analysis was used for calculation of Langelier, Ryznar and Puckorius indices for the purpose of an influence of water chemical parameters on the corrosion effect of the pipe line [6-11].

Preparation of galvanized steel pipe samples for microscopic analysis was performed according to ASTM E3-11: 2017 [12]. The samples were examined using optical microscope:

- Nikon equipped with video camera Nikon DS-2 16 MP and objectives Nikon TU Plan Fluor 10×/0.30 and Nikon TU Plan Fluor 100x/0.90.

3. Results and Discussion

3.1. Measurement of hot water supply pipeline voltage in a building

A random AC voltage measurement result is recorded (Fig. 2). Figure 2 shows the dependence of the voltage magnitude (y axis) over time (x axis). The time scale starts at 0, and cell 1 corresponds to 1 second. The AC voltage scale is shown in the range from -500mV to + 500mV, 1 cell of the graph corresponds to 100mV. The measured signal (blue) is similar to noise. It was observed that most of the signal amplitude is on the negative side of the signal. This proves that an alternating voltage current is induced in the pipeline. The generated voltage is not constant, it jumps from the minimum amplitude value (black dotted line in Fig. 2) to the maximum (highest rising peaks on the positive and negative sides of the vertical axis).

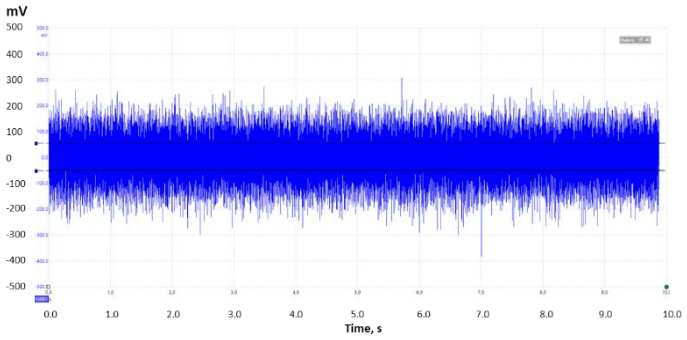


Fig. 2. *A voltage measurement of about 10 seconds was recorded when the Picoscope 3424 portable computer oscilloscope was connected to the hot water supply pipeline and the ground terminal of the power outlet installed in the building*

After processing the measurement results, taking into account the electrical signal noises generated by the ground circuit and eliminating them from the measurement curves, it was determined that the amount of alternating current in the hot water supply pipeline is about 20-60 mV (measured indoors). At the heating point, the hot water pipeline was grounded through a frame structure, i.e. through mounted brackets to secure the pipes. However, the hot plumbing structure has screw fittings. These connections use non-conductive insulating materials that block the flow of water to the outside, so as one moves away from the heat point, the grounding resistance of the pipeline increases due to the deteriorating contact (pipe-connection-pipe) (measured in the room is about 0.1 Ω).

It was observed that the predominant frequency of the electric field is unstable. It can be assumed that such frequencies are generated not only by disordered electrical equipment installed in the pipeline, but also by various other components in the environment (e.g. magnetic fields, radio frequency waves, etc.).

3.2. Influence of the chemical composition of hot water on the corrosion of steel pipe

According to the data of scientific literature, corrosion of metals can be promoted by the concentration of dissolved oxygen in water, pH, water hardness, concentration of HCO_3, Cl^-, SO_4 ions, temperature (special influence of temperature in closed systems, then corrosion in steel can reach about 0.25 mm/year at 40°C, and at 80°C - ~ 0.5 mm/year [13]) and other factors [1, 14]. The influence of water temperature on the dissolution of zinc coating is shown in Fig. 3. The figure shows that corrosion of zinc accelerates greatly when the water temperature rises above about 50°C.

The water temperature was measured by turning off the hot water tap. Measured value was 59°C. According to scientific articles [1, 4, 13], when the water temperature is 50-80°C, the probability of corrosion in galvanized pipes increases significantly.

The chemical composition and other properties of the relevant components of hot water samples were tested in an accredited laboratory. Chemical Research Protocol No. Data for Ch 5082/2020 is presented in Table 1. This study identified the amounts and properties of chemical elements and compounds that may affect or promote corrosion in the pipeline.

After determining the amounts of chemical elements and compounds that can effect on metal corrosion, calculations were performed according to various methodologies found in the literature [6-11, 15] in order to find out the properties of water flowing through the studied pipeline. The chemical properties of water are described by parameters such as: water hardness (Ca and Mg in the water), alkalinity of the water (HCO_3 and CO_3 in the water), Langelier index (determining whether the water is chemically balanced, promoting corrosion or decomposition of lime), Saturation index (determining whether the water is saturated with $CaCO_3$ or not), the Ryznar Stability Index (determining whether the water supplied promotes corrosion or limescale decomposition), the Puckorius Stability Index (determining whether there is a tendency to lime decomposition or corrosion) and the Larson Index (determining whether corrosion is encouraged). An explanation of the above characteristics and values of the hot water sample is given in Table 2. The results show that the Ryznar and Puckorius indices show the effect of water on the formation of pipe corrosion.

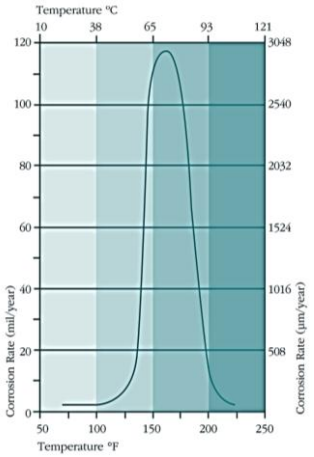


Fig. 3. *Influence of water temperature on zinc corrosion* [4]

Table 1: *Test results for water samples*

Analyst	Result	Measurement unit	Allowed until (HN 24: 2017)
Magnesium	< 1	mg/l	Unregulated
Calcium	< 2	mg/l	Unregulated
Total hardness	0.06	mmol/l	Unregulated
Chloride content	47	mg/l	250.0 mg/l
pH	8.2	when T =20.2°C	6.5 – 9.5
Specific electrical conductivity	667	μS/cm, when T =25.4°C	2500 μS/cm, when T=25°C
Total alkalinity	4.93	mmol/l	Unregulated
Hydrocarbonate content	301	mg/l	Unregulated

Table 2: *The results of the performed calculations according to the methodologies* [6-11, 15]

Parameter	Result of calculation	Measurement unit	Galvanized pipe susceptibility to corrosion under the existing parameter
Water hardness	9.10	mg $CaCO_3$/l	Yes
Alkalinity of water	246.91	mg $CaCO_3$/l	-
Langelier Index of corrosive media (LSI)	-0.04	-	No
Saturation Index (SI)	-0.05	-	No
Ryznar Stability Index (RSI)	8.27	-	Yes
Puckorius Stability Index (PSI)	8.43	-	Yes
Larson Index (LaI)	0.3	-	No

Corrosion of galvanized steel pipes is also promoted by water softening [3]. Water softening facilities are installed in the building where the test pipe was operated.

The hardness of water is determined by calcium and magnesium compounds, which are important for human health and give water its flavor. When hard water is heated, calcium carbonate also settles on the pipe walls, accumulating a layer of lime. By softening the water, calcium and magnesium are removed and replaced with sodium (and sometimes potassium). Softened water is actually

aggressive (corrosive) to carbon steel and galvanized steel. The zinc coating on the steel pipe is largely protected by a layer of zinc carbonate forming on the surface. A certain hardness (calcium carbonate content) in the water is beneficial because it helps to form a protective layer. In addition, a thin layer of calcium carbonate and zinc carbonate is more resistant to corrosion than zinc carbonate alone in fully softened water. When the hardness is greatly reduced, the protective layer does not form properly and the zinc coating is susceptible to corrosion. For this reason, the zinc coating primarily acts as an anode, i. dissolves. However, when the zinc is completely gone, the steel pipe itself begins to corrode and the iron corrosion waste enters the water. All these processes are driven by water heating [3].

As we can see from the hot water chemical study of the building and based on the work of other scientists, we can say that galvanized steel pipes are not the right choice to supply hot water.

3.3 Microscopic examination of samples of galvanized steel pipes used for hot water supply in a building

Electrochemical corrosion occurs in electrolyte solutions or in a humid atmosphere. During it, a very large number of corrosive galvanic cells are formed at the point of contact between the metal surface (in this case the pipe or other parts of the pipeline) and the electrolyte (water with dissolved chemical elements). Anodic and cathodic areas are formed on the metal surface, between which a potential difference occurs and an electric current flows.

The two metals, joined together and surrounded by an electrolyte (water), form a galvanic pair. One of them will start to dissolve (become an anode) at the expense of the other (become a cathode). The anode will be the one whose electrode potential is more negative. Thus, in the iron-zinc pair, the zinc will dissolve, and then iron corrosion will begin. Due to the high temperature, the chemical elements dissolved in the water, intense corrosion took place in the zinc-iron pair, where the electrolyte (hot water) was involved in the chemical reactions. After cutting the samples of the operated pipes, continuous corrosion was found with large accumulations of corrosion products occurring in places (Fig. 4).



Fig. 4. *Internal surfaces damaged by corrosion of the test tube*

Selected sites for microscopic analysis are corrosion-damaged sites and possibly the least corrosion-affected site for comparison.

According to ISO 14713-1 [14], the minimum zinc coating inside the pipe for zinc-coated pipes must be 55µm. In order to estimate the thickness of the zinc coating, the least corrosion-damaged areas were searched. In some places, the thickness of the zinc coating in the inner layer was found to exceed 100 µm, which means that the thickness of the zinc coating was at least twice the minimum allowable thickness according to ISO 14713-1 [14] (Fig. 5).

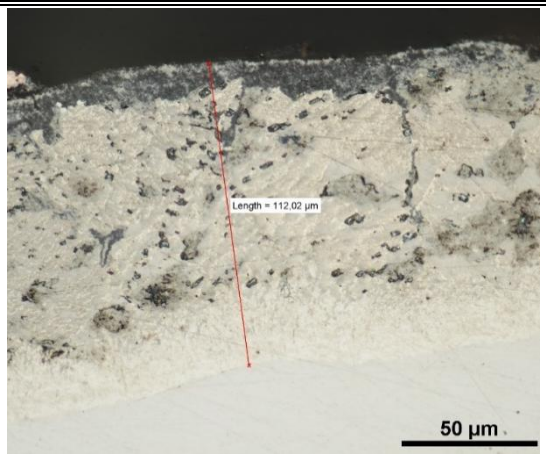


Fig. 5. *Microstructure of the inner surface of the test pipe. No blisters, pores or other defects are visible on the zinc coating and the steel boundary*

By studying the microstructure of the tube samples, several emerging holes were found (Fig. 6). There was very little material left at some of the holes until complete rusting. Holes formed in the coating due to corrosion, which may have had a channel to the outside, were also found (Fig. 7).

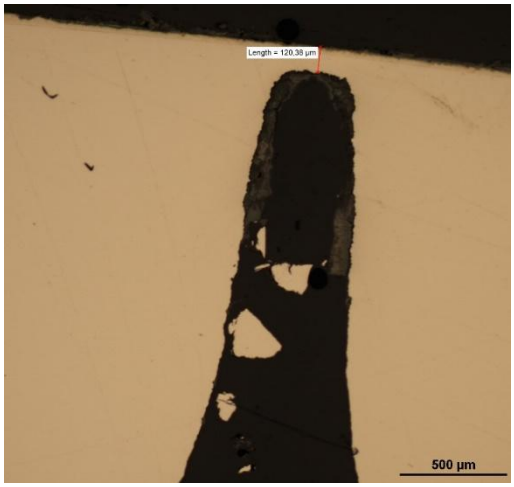


Fig. 6. *Corrosion holes in the test tube (from the inner surface to the outside)*

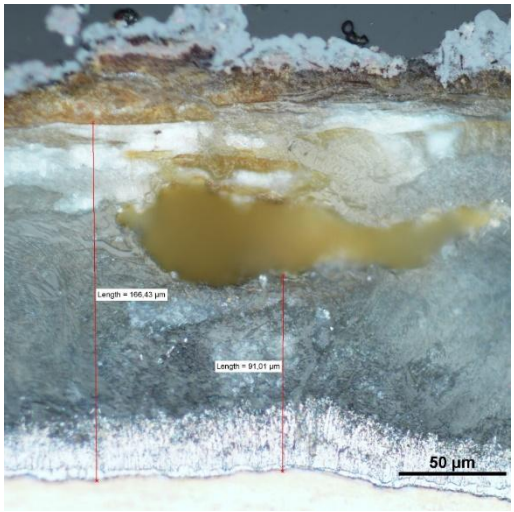


Fig. 7. *Holes in the zinc coating of the inner surface of the test tube due to corrosion*

4. Conclusions

Voltage measurements revealed the occurrence of stray electrical currents in the hot water supply pipes. It was found that the voltage of the alternating current in the hot water supply pipeline is about 20-60 mV. Stray electrical currents are one of the causes of electrochemical corrosion.

A chemical test for hot water was performed at the National Public Health Laboratory, Lithuania. Based on the obtained chemical composition, the Langelier and Ryznar indices were calculated, which showed that the chemical composition of hot water flowing in a building promotes corrosion of zinc-coated pipes. The scientific literature sources mention that corrosion intensifies particularly at temperatures above 50°C. To prevent corrosion, it is recommended to select materials and coatings according to EN ISO 14713-1 for all structural components (including pipes, fittings, tanks and tank lids) that come into contact with drinking water. According to the said standard, galvanized pipes are most suitable for use in atmospheric corrosion conditions. It has also been found in the literature that water softening promotes corrosion of galvanized pipes.

When examining samples of the test pipe by metallography, the thickness of the zinc coating meets the requirements of the standard EN ISO 14713-1. Hole rust sites were formed, forming deep holes due to corrosion.

5. References

1. A. Andrianov, D Spitsov. Corrosion of galvanized pipes in the hot water supply system, MATEC Web of Conferences 106, 03028, 2017.

2. M. Carbucicchio, R. Ciprian, F. Ospitali, G. Palombarini. Morphology and phase composition of corrosion products formed at the zinc–iron interface of a galvanized steel. Corrosion Science, Vol. 50 p. 2605–2613, 2008.

3. C. Noble. Corrosion of Galvanized Piping in Domestic Water Systems. The Conduit, Vol. 12, No. 1, p. 1-3, 2013.

4. Corrosion resistance of zinc in water. Corrosion Technical Bulletin 5, May 2019. Revision 5.

5. S. Goidanich. Influence of Alternating Current On Metals Corrosion, Ph.D. Thesis in Materials Engineering, 160 p., 2002-2005.

6. W. F. Langelier. The analytical control of anti-corrosion water treatment, Journal of the American Water Works Association, Vol. 28, Iss. 10, pp 1500-1521, 1936.

7. W. F. Langelier. Chemical equilibria in water treatment, Journal of the American Water Works Association, Vol. 38 Iss. 2, p. 169-178. 1946.

8. 2330-B Standart Methods for the Examination of Water and Wastewater.

9. J. W. Ryznar. A new index for determining amount of scale formed in water, Journal of the American Water Works Association, Vol. 36 Iss. 2, p. 472-486, 1949.

10. R. Puckorius, J. M. Brooke. A new practical index for calcium carbonate scale prediction in cooling system, corrosion, p. 280-284, April 1991.

11. P. R. Puckorius, G. R. Loretitsch. Cooling water scale and scaling indices: what they mean – how to use them effectively – how they can cut treatment costs, Paper IWC-47, International Water Conference, Pittsburgh, PA, 1999.

12. ASTM E3-11:2017. Standard Guide for Preparation of Metallographic Specimens, ASTM International, West Conshohocken, PA, 2017, www.astm.org.

13. A. Šulčius. Corrosion of Metals. Kaunas: Technologija p. 212, 1995 [in Lithuanian].

14. ISO 14713-1:2017, Zinc coatings — Guidelines and recommendations for the protection against corrosion of iron and steel in structures — Part 1: General principles of design and corrosion resistance.

15. T. E. Larson, R. V. Skold. Laboratory Studies Relating Mineral Quality of Water to Corrosion of Steel and Cast Iron (1958) Illinois State Water Survey, Champaign, IL pp. 43-46: ill. ISWS C-71.

Recent applications of nanoparticles in wood-based panels

Nadir Ayrilmis
Department of Wood Mechanics and Technology, Forestry Faculty, Istanbul University, Bahcekoy, Sariyer, 34473, Istanbul, Turkey
nadiray@istanbul.edu.tr

Abstract: *Nanocellulose applications in the wood-based panels have gained a great deal in the scientific researches and industrial applications. Utilization of natural and synthetic nanoparticles as reinforcement in the wood-based panels has considerably increased in the last two decades due to their unique properties. The main property of the nanocellulose is its very high surface area. Hereby, the very small use of nanoparticles suh as %1-2 wt% in the composites is enough at a relatively low-cost. Nanoparticles are presently considered to be high-potential reinforcing fillers for the enhancement of the physical, mechanical, electrical/electronic properties, thermal resistivity, fire, durability properties of wood-based panels such as particleboard, fibreboard, oriendted strandboard, and plywood. The nanoparticles are applied to wood based panels during the manufacture and after production. The raw materials such as wood or resin can be treated with nanoparticles or the finished panels can be treated with nanoparticles. In this study, the recent developments in the nano particles, their applications in the wood based panels, and their effects on the panel properties were reviewed.*
KEYWORDS: *NANOFILLER, WOOD-BASED PANEL, RESIN, MECHANICAL PROPERTIES, PHYSICAL PROPERTIES*

1. Introduction

Nanotechnology is defined as the manipulation of particles between 1 and 100 nm. The great developments were achived in the industrial applications of nano fillers in last two decades. Utilization of nanofillers have recently increased in wood and wood based panel industry. The aim of the addition of the nanoparticles into the wood and wood-based panel is to develop new and improved materials with significant functions, physical and chemical properties. The largest commercial applications of nanofillers are in the lightweight and high-strength composites. The nano fillers can be applied to the wood based panels in different ways such as addition into the resin, treatment with wood particles or fibers, addition to the sırface coatings. Especially, surface applications of nanofillers are practical and easier as compared to other applications. The use of nanofillers in the coatings of wood and wood-based panels may improve water repellency, biological durability, antibacterial property, and fire resistance. Physical, mechanical, surface, barrier, and optical properties of polymeric coatings can be improved by nanoparticles of different shapes such as spheres, tubes, rods, and others. Nanosized materials like metal nanoparticles (silver, gold, copper…), metal oxides (zinc oxide, aluminum oxide…), clays etc., are widely used to achieve these improvements [1]. The hydrophobic character of the wood after the the application of coating with the nanofillers is presented in Figure 1.



Fig. 1*: Water repellency of wood after the application of coating with the nanofillers [2].*

Figure 2 shows that nanocellulose did not show any negative effect on the on the glossiness of waterborne polyurethane paint film. Nanocellulose has ultra-fine size, high aspect ratio, rich active functional groups, and a network structure [3].

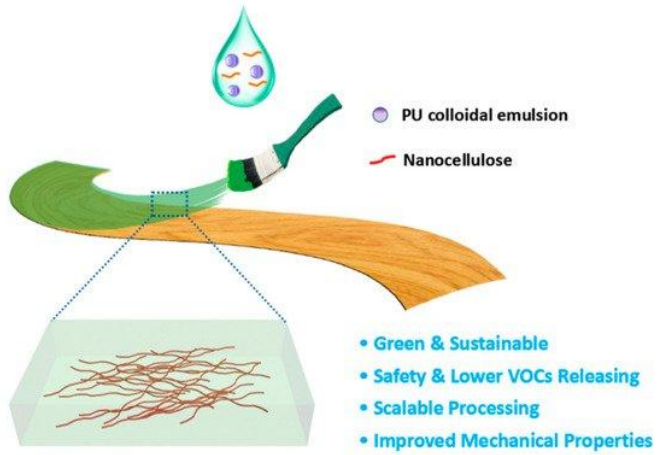


Fig 2: *Schematic illustrations of nanocellulose-reinforced waterborne polyurethane as wood coating [3].*

A general classification of nanofillers are presented in Figure 2.

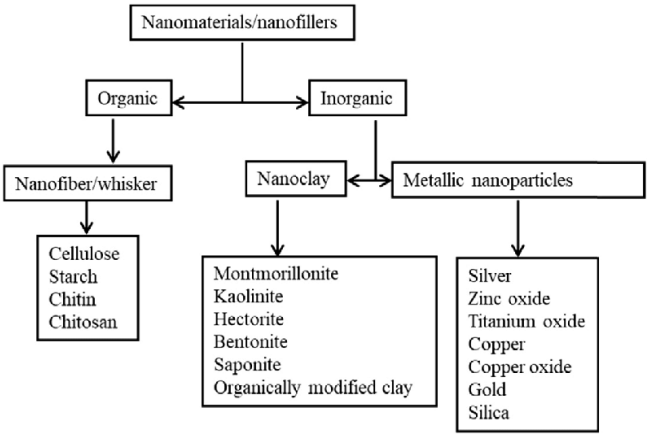


Fig. 2: *Classification of nanofillers [4].*

2. Applications of inorganic nanofillers in the wood-based panel industry

Inorganic nanofillers have been used in wood-based panel industry for a couple of decades. In addition to the academic and industrial applications, there are also patents on the use of nanofillers in the wood-based panel industry. For example, Wang and Xing [5] developed wood adhesives containing the reinforced additives for structural engineering products. They patented (WO2009086141A) the use of any type of nanocellulose, nanocarbon, and nanoclay in any type of wood adhesive (UF, MUF, PF, MUPF, pMDI, protein, epoxy etc.)

at various ratios for the production of various types of wood-based panels. They reported nanomaterial and micromaterial additives improved the structural properties of adhesives and mostly the mechanical properties of the panels.

Park and Lee [6] investigated the production of E0 grade UF using titanium dioxide scavenger at 0.5%, 1%, and 3 wt% based on the oven dry weight of UF resin. The results showed that the 1 wt% addition of titanium dioxide did not a significant effect on the mechanical and physical properties of the particleboards produced with the E0 type UF resin but further increment in the titanium dioxide content decreased the mechanical properties. Costa et al. [7] investigated the effects of sodium metabisulfite, ammonium bisulfite, and urea on the technological properties and formaldehyde emission of particleboard. Among the scavengers, the sodium metabisulfite was the best additive giving the particleboards with zero formaldehyde emission. Dudkin et al. [8] added aluminum oxide nanoparticles in the UF resin to decrease the free-formaldehyde. Kızılkaya et al. [9] investigated that the physical and mechanical properties of medium density fiberboards (MDF) produced with urea formaldehyde adhesive reinforced with nano-boron nitride (BN) and nano-titanium dioxide (TiO_2). The addition of 0.5% and 1.5% nano particles into the UF resin improved the mechanical properties of the MDF panels. The thermal stability of urea formaldehyde adhesive with TiO_2 is increased and maximum mass loss temperatures are higher than the addition of nano-BN. It was concluded that the adding nano-particles had a positive effect on the physical and mechanical properties of the MDF panels. Candan and Akbulut [10] investigated the physical and mechanical properties of nano-reinforced particleboards. The results showed that the incorporation of nanomaterial significantly improved the physical and mechanical properties of the particleboards.

In a previous study, it was found that the addition of nano-SiO_2 into the urea formaldehyde resin improved the adhesive bond quality and the hardness of wood [11]. In another study, Chen et al. [12] studied the properties of fiberboard based on nano-lignocelluloses/$CaCO_3$/PMMA composite. They reported that the composites materials had good mechanical, dimensional stability, and thermal properties which improved when the nano filler loading was increased.

Kumar et al. [13] produced MDF panels with multiwalled carbon nanotubes (MWCNT) using UF resin. The response surface methodology was employed to optimize the relationship between the three variables which were pressing time, percentage of UF resin and percentage of MWCNT. The optimum conditions based on the internal bond strength were determined as 8.18% of UF resin, pressing time of 232 s, and MWCNT of 3.5%.

The effect of alumina (Al_2O_3) nanoparticles on the physical and mechanical properties of MDF panels was investigated by Alabduljabbar *et al.* [14]. . The nanoparticles were added into the UF resin with different loading levels, 1.5%, 3%, and 4.5% by weight, respectively. The results showed that the properties of the MDF panels with nano filler were better than those of the control MDF panels. The results also revealed that increasing alumina nanoparticles in the UF resin positively affected the mechanical properties of the MDF panels

Iždinský et al. [15] studied the influence of zinc-oxide and silver nanoparticles in acrylic coatings applied to the surface particleboard and MDF. It was concluded that the antibacterial resistance of the panels was higher if these composites contained a higher amount of formaldehyde due to contact with water or humid environments.

Valle et al. [16] investigated the influence of SiO_2 nanoparticles on the mechanical and physical properties of particleboard. SiO_2 nanoparticles were added to UF resin. The results showed that the combination of SiO_2 nanoparticles and UF resin improved the resistance to thickness swelling by 42% and thus enhanced the dimensional stability of the particleboard.

Gul et al. [17] investigated the influence of iron oxide (Fe_2O_3) nanoparticles on the physical properties of MDF panels. Three different loading levels of nano ironoxide (0.5, 1.5, and 2.5 wt%) were used in the experiments. It was determined that the addition of homogeneously dispersed iron oxide nanoparticles significantly improved thickness swelling. The curing temperature and thermal stability of the resin improved due to the addition of Fe_2O_3 nanoparticles. The presence of iron oxide nanoparticles in an epoxy polymer contributed to a stiffer matrix that, effectively, enhanced the capability of improving the physical properties of the MDF panels.

Chotikhun et al. [18] determined the formaldehyde emission and mechanical properties of the particleboards produced from Eastern redcedar using silicone dioxide (SiO_2) nanoparticles added modified starch as a binder. Nine different types of panels were manufactured having nanoparticle contents of 0%, 1%, and 3% at three density levels of 600, 700, and 800 kg/m^3. The results showed that the nanoparticle content above 1% adversely affected the mechanical properties of the particleboard. Very low formaldehyde emission value of 0.07 ppm was determined for the particleboards.

3. Applications of organic nanofillers in the wood-based panel industry

The utilization of organic nanofillers has considerably increased in last decade, especially cellulose nanofibers (CNFs). Generally, there are two representative CNFs, nanocrystalline cellulose (NCC) and microfibrillated cellulose (MFC). NCC is generally prepared by acid hydrolysis under strict conditions and has high crystallinity and low aspect ratio. The product, microfibrillated cellulose (MFC), exhibits gel-like characteristics. NCC suspensions have liquid-crystalline properties. A third nanocellulose variant, bacterial nanocellulose (BNC), is prepared from low-molecular-weight resources, such as sugars, by using acetic acid bacteria of the Genus *luconacetobacter* [19].

Use of nanocelluloses as reinforcements in adhesives for the production of reconstituted wood panels has several benefits such as possibility of altering the properties of adhesives, gain in mechanical and physical properties of panels and reduction in formaldehyde emissions by panels using synthetic adhesives [20]. Veigel et.al [21] added the CNFs in the UF and MUF resin at of 0, 1, and 3 wt% contents of the CNFs. They were prepared by mixing an aqueous CNF suspension with UF and MUF adhesives. The particleboards and oriented strand boards (OSBs) were produced under laboratory conditions. Particleboards prepared with UF + 1 wt% CNF showed reduced thickness swelling, better internal bond and bending strength than boards produced with pure UF. The reinforcing effect of CNF was even more obvious for OSB where a significant improvement of strength properties of 16% was found.

Table 1. *The family of nanocellulose materials [22].*

Type of nano cellulose	Selected reference and synonyms	Typical sources	Formation and average size
Microfibrillated cellulose (MFC)	Microfibrillated cellulose, nanofibrils and microfibrils, nanofibrillated cellulose	Wood, sugar beet, potato tuber, hemp, flax	Delamination of wood pulp by mechanical pressure before and/or after chemical or enzymatic treatment diameter: 5–60 nm length: several micrometers
Nanocrystalline cellulose (NCC)	Cellulose nanocrystals, crystallites, whiskers, rodlike cellulose microcrystals	Wood, cotton, hemp, flax, wheat straw, mulberry bark, ramie, Avicel, tunicin, cellulose from algae and bacteria	Acid hydrolysis of cellulose from many sources diameter: 5-70 nm length: 100-250 nm (from plant celluloses); 100 nm to several micrometers (from celluloses of tunicates, algae, bacteria)
Bacterial nanocellulose (BNC)	Bacterial cellulose, microbial cellulose, biocellulose	Low-molecular-weight sugars and alcohols	Bacterial synthesis diameter: 20-100 nm; different types of nanofiber networks

Atta-Obeng et al. [23] added microcrystaline cellulose (MCC) in phenol-formaldehyde resin at the levels of 0, 3, 6 and 10 wt% (wt/wt).and then tested their thermal and shear strength properties. Their results showed a viscosity increase and a slight reduction of the curing temperature by 4°C. The heat of reaction was a function of cellulose loading with the maximum heat of reaction occurring at 3 wt% loading. The shear strength of the PF adhesive was increased by a factor of 1.7 with a 10% cellulose loading.

Atta-Obeng [24] produced particleboards from the wood particles of sweet gum and pine trees and phenol-formaldehyde resin. The addition of 10% nanocrystaline cellulose decreased the mechanical properties, increased thickness swell and decreased spring back. Cellulose reinforcement lowers the cure temperature as well as the thermal stability of the neat PF adhesive. Lap shear tests revealed an increase in shear strength with the addition of cellulose.

As known, the formaldehyde emission is one of the most important issues in wood-based panel industry. The researchers focus on the decreasing formaldehyde emission from the wood-based panels. In literature, there are plenty of experimental studies on decreasing formaldehyde emission from wood-based panels such as plywood, oriented strand board, particleboard, MDF. For example, Cademartori et al. [25] added small percentages of aluminium oxide nanoparticles into UF resin and investigated thermo-mechanical properties of the composites. They reported that aluminium oxide nanoparticles were effective to reduce the formaldehyde emission (14%) from MDF based on the results of the desiccator test. Ayrilmis et al. [26] modified super E0, E0, and E1 grade UF resins using microfibrillated cellulose (5 wt%). The laminated veneer lumbers (LVLs) were produced from the unmodified and modified SE0, E0, and E1 grade resins. The total volatile organic compounds (TVOC) and HCHO of the LVLs were determined at 25 °C, 35 °C, and 45 °C for 30 min using a thermal extractor. The total volatile organic compounds (TVOCs) from wood-based panel considerably decreased with increasing amount of MFC.

Ayrilmis et al. [27] investigated that the relationship between urea–formaldehyde (UF) adhesives (E0 and E1 classes) and microfibrillated-cellulose (MFC) and its effect on the mechanical properties of laminated veneer lumbers (LVLs) were investigated. The tensile shear strength of the LVLs significantly increased (2.89 to 3.35 N/mm^2) as the MFC suspension was increased to 3.75 g in the 7.50 g E0 class UF adhesive, while it slightly increased (3.10 to 3.16 N/mm^2) as the MFC suspension was increased to 2.5 g in the 8.75 g E1 class UF adhesive. The MFC was found to be valuable nanoscale reinforcing filler for the improvement of bond performance of UF adhesive, in particular, E0 class adhesive, in the production of wood-based composites.

Nanocellulose is known to form an airtight film on the surface of wood and various other small particles such as pigments. This makes nanocellulose-based coatings highly suitable for the protective treatment of wood surfaces. VTT (Technical Research Centre of Finland Ltd.) scientists have developed a new nanocellulose coating to protect wood-based materials from fire (Fig. 3).

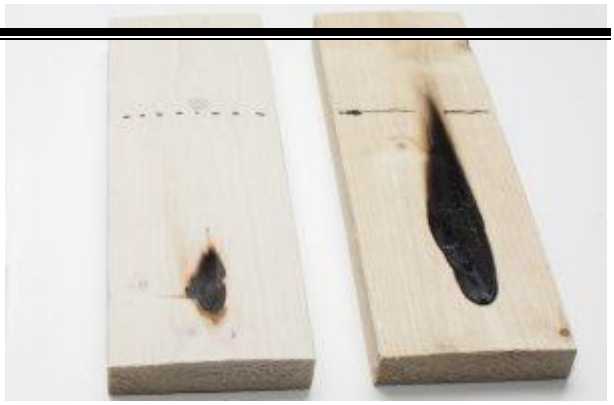


Fig. 3: *Nanocellulose coating protects wood-based materials from the fire.*

4. Conclusions

This study summarized recent applications of nanofillers in the wood-based panels. The improvements in the dimensional stability, surface properties, formaldehyde emission, mechanical properties, biological durability of the panels were determined. Furtheremore, the modification of the wood resins which improves the resin properties was efficiently carried out in the studies. Nanofillers have unique properties to improve physical, mechanical, and thermal properties of wood-based panels. It is expected that the utilization of the nanofillers as reinforcement in the wood-based panels, particularly nanocellulose will considerably increase in near future.

5. References

1. Nikolic M, Lawther JM, Sanadi AR. Use of nanofillers in wood coatings: a scientific review. *J Coat Technol Res* **12,** 445–461 (2015).
2. Anonymous. Super hydrophobic coating changes wood ınto waterproof wood. https://ultrahydrophobiccoating.com/product/super-hydrophobic-coating-changes-waterproof-wood/
3. Kong L, Xu D, He Z, Wang F, Gui S, Fan J, Pan X, Dai X, Dong X, Liu B, Li Y. Nanocellulose-Reinforced Polyurethane for Waterborne Wood Coating. *Molecules*. 2019;24(17):3151.
4. Shankar S, Rhim JW. Bionanocomposite Films for Food Packaging Applications. Reference Module in Food Science, 2018
5. Wang S, Xing C. Wood adhesıves containing reınforced additives for structural engineerıng products. US patent no: US20160115359A1, US patent Office.
6. Park HS, Lee HH. A novel manufacturing method of urea-formaldehyde resin with the titanium dioxide for reducing formaldehyde emission. Jour Agri Sci 2009;36:11-18
7. Costa NA, Pereira J, Ferra J, Cruz P, Martins J, Magalhaes FD, Mendes A, Carvalho LH. Scavengers for achieving zero formaldehyde emission of wood-based panels. Wood Sci Technol 2013;47:1261-1272.
8. Dudkin, BN, Krivoshapkin VP, Krivoshapkina EF. Effect of aluminum oxide nanoparticles on the properties of urea-formaldehyde resin. Russ. J. Appl. Chem. 2006;79:1522–1525.
9. Kızılkaya A, Aydemir D, Onat SM, İstek A. Effects of different nano fillers on the physical and mechanical properties of medium density fiberboards (MDF). Journal of Bartin Faculty of Forestry 2020; 22 (3):878-885.
10. Candan Z, Akbulut T. Physical and mechanical properties of nanoreinforced particleboard composites. Maderas. Ciencia y tecnología, 2015;17(2):319-334.
11. Jiang Y, Wu G, Chen H, Song S, Pu J. Preparation of Nano-SiO2 Modified Urea-Formaldehyde Performed Polymer to Enhance Wood Properties. Rev.Adv. Mater. Sci. 2013;33:46-50.
12. Chen Y, Cai T, Dang B *et al.* The properties of fibreboard based on nanolignocelluloses/$CaCO_3$/PMMA composite synthesized through mechano-chemical method. *Sci Rep* 2018;**8:**5121.

13. Kumar A, Sharma KV, Gupta A et al. Optimization of processing parameters of medium density fiberboard using response surface methodology for multiwalled carbon nanotubes as a nanofiller. Eur. J. Wood Prod. 2017;75:203–213.
14. Alabduljabbar H, Alyousef R, Gul W, Shah SRA, Khan A, Khan R, Alaskar A. Effect of Alumina Nano-Particles on Physical and Mechanical Properties of Medium Density Fiberboard. Materials, 2020;13(18):4207.
15. Iždinský J, Reinprecht L Nosál E. Antibacterial efficiency of silver and zinc-oxide nanoparticles in acrylate coating for surface treatment of wooden composites. Wood Res. 2018;63:365-372.
16. Valle ACM, Ferreira BS, Prates GA, Goveia D, De Campos CI. Physical and mechanical properties of particleboard from eucalyptus grandis produced by urea formaldehyde resin with SiO_2 nanoparticles. Eng. Agríc. 2020;40:289-293.
17. Gul W, Alrobei H, Shah SRA, Khan A. Effect of iron oxide nanoparticles on the physical properties of medium density fiberboard. Polymers, Dec;12(12).
18. Chotikhun A, Hiziroglu S, Buser M, Frazier S, Kard B. Characterization of nano particle added composite panels manufactured from Eastern redcedar. Journal of Composite Materials 2018;52(12):1605–1615
19. Ayrilmis N. Nanocellulose as a green and sustainable material for biocomposite industry. 2th International Conference on Technology and Science, 14-16 November 2019, Mehmet Akif University, Burdur, Turkey.
20. Lengowski EC, Júnior EAB, Kumode MMN, Carneiro ME, Satyanarayana KG. Nanocellulose-reinforced adhesives for wood-based panels, sustainable polymer composites and nanocomposites. Springer International Publishing, 2019.
21. Veigel S, Rathke J, Weigl M, Gindl-Altmutter W. Particleboard and oriented strand board prepared with nanocellulose-reinforced adhesive. Journal of Nanomaterials. 2012
22. Ayrilmis N, Ashori A. Alternative solutions for reinforcement of thermoplastic composites. In: Natural Fiber Composites ed. R.D.S.G. Campilho (Boca Raton: CRC Press, 2015.
23. Atta-Obeng E, Via B, Fasina O. Effect of microcrystalline cellulose, species, and particle size on mechanical and physical properties of particleboard. Wood and fiber science, 201:44:227-235.
24. Atta-Obeng E (2011) Characterization of phenol formaldehyde adhesive and adhesive-wood particle composites reinforced with microcrystalline cellulose. MSc thesis, Auburn University
25. de Cademartori PHG, Artner MA, de Freitas RA, Magalhaes WLE. Alumina nanoparticles as formaldehyde scavenger for urea-formaldehyde resin: rheological and in-situ cure performance. Compos B Eng 2019;176:107281
26. Ayrilmis N, Lee YK, Kwon JH, Han TH, Kim HJ. Formaldehyde emission and VOCs from LVLs produced with three grades of urea-formaldehyde resin modified with nanocellulose, Building and Environment, 2016;97:82-87,
27. Ayrilmis N, Kwon JH, Lee SH, Han TH, Park CW (2016) Microfibrillated-cellulose-modified urea-formaldehyde adhesives with different F/U molar ratios for wood-based composites, Journal of Adhesion Science and Technology, 2016;30:2032-204